Sebastian Peterka, BSc

Development of humidity sensors based on hydrogels deposited by initiated chemical vapor deposition

MASTER'S THESIS

to achieve the university degree of

Diplom-Ingenieur

Master's degree programme: Technical Physics

submitted to

Graz University of Technology

Supervisor

Ass.Prof. Dr. Anna Maria Coclite

Institute of Solid State Physics

Graz, April 2018

AFFIDAVIT

I declare that I have authored this thesis independently, that I have not used other than the declared sources/resources, and that I have explicitly indicated all material which has been quoted either literally or by content from the sources used. The text document uploaded to TUGRAZonline is identical to the present master‘s thesis.

Date

Signature

ACKNOWLEDGMENTS

First of all I want to thank my supervisor Ass.Prof. Anna Maria Coclite for her support and guidance throughout this thesis.
She and Alberto Perrotta always had time for my questions, provided their knowledge, were always motivating and showed understanding regarding the time I needed for my self employment.

Furthermore I want to thank the whole CVD-ALD group, including Paul Christian, Sarah Dörschlag, Marianne Kräuter, Fabian Muralter, Julian Pilz, Paul Salzmann, Stephan Tumphart and Katrin Unger for their help, their input and the great working atmosphere the last year.

Special thanks also go to the Institute of Electron Microscopy and Nanoanalysis (FELMI), Graz University of Technology, (Steyrergasse 17, 8010 Graz, Austria), especially to Prof. Ferdinand Hofer, enabling the use of the (E)SEM and Dr. Armin Zankel for his help and acquiring the (E)SEM data used in this thesis, also to the Montanuniversität, Prof. Christian Teichert and Caterina Czibula, for their help with the AFM measurements and Prof. Peter Hadley for showing me how to use the in-house SEM.

Also my friends, who were always there for me and guided me through the last years, my studies and this thesis, deserve to be mentioned.

Last but no least I would like to thank my parents Sissi and Konrad Peterka for their never ending support in all regards, their love in everything I do and being there for me, no matter what happens.

ABSTRACT

In this thesis the use of hydrogel films as a material for humidity sensors in low humidity environments like natural gas pipeline systems was investigated. A hydrogel is a stimuli-responsive polymer network, which can absorb and retain water (vapour) due to its hydrophilic pedant functional groups, which means, that an increase of volume with the uptake of water can be observed. This polymer thin films were synthesized by initiated chemical vapour deposition (iCVD) which allows, due to the vapour-phase nature of its process, the coating with uniform thin-films with a controlled material composition.
Various planar thin films with co-polymeric compositions using 2-Hydroxyethyl methacrylate (HEMA), as the main monomer, methacrylic acid (MAA), and ethylene glycol dimethacrylate (EGDMA) as a cross-linker have been synthesized. The increase in volume of a thin film is constrained by the attachment to the surface from which it is grown. [1] To enhance the degree of swelling the use of nanostructures, in form of nano-tubes, was attempted in addition to planar films.
The so prepared polymer films were analysed by spectroscopic ellipsometry, atomic force microscopy, (environmental) scanning electron microscopy and energy dispersive x-ray spectroscopy, to investigate their uniformity, topography, swelling behaviour and chemical composition.
It was found that pHEMA polymer films do have a sufficient response in thickness when analysed with spectroscopic ellipsometry and can therefore be used in low humidity environments and for humidity sensing in natural gas. The successful synthesis of p(HEMA-co-EGDMA) nano tubes, using anodic aluminium oxide membranes as templates can be shown.

KURZFASSUNG

In dieser Arbeit wurde die Verwendung von Hydrogeldünnschichtfilmen als Ausgangsmaterial für Feuchtigkeitssensoren in Umgebungen mit sehr niedrigen Feuchtigkeitswerten, wie sie zum Beispiel in Erdgasleitungen zu finden sind, untersucht. Ein Hydrogel ist ein Netzwerk bestehend aus stimuli-responsiven Polymerketten, welche Wassermoleküle reversibel binden können durch die hydrophilen funktionellen Gruppen der verwendeten Monomere. Dadurch kann eine Vergrößerung des Volumens, welche in Relation zum Wassergehalt steht, beobachtet werden. Die verwendeten Polymerdünnschichtfilme wurden per radikalinitiierter chemischer Gasphasenabscheidung synthetisiert, welche durch ihre Gasphasennatur im zugrundeliegenden Prozess die Beschichtung einer Probe mit homogenen Dünnschichtfilmen gewünschter Zusammensetzung erlaubt.
Dabei wurden Copolymere unterschiedlicher Zusammensetzung unter Verwendung von 2-Hydroxyethylmethacrylat (HEMA), als Hauptmonomer, Methacrylsäure (MAA) und Ethyleneglykoldimethacrylat (EGDMA) als Crosslinker synthetisiert. Die Volumenszunahme eines Dünnschichtfilms wird durch die Bindung an die Oberfläche, auf welcher er wächst, gehemmt. Um den Grad des Anschwillens eines solchen Polymerfilms zu erhöhen wurde durch Nanostrukturierung in Form von Nanoröhrchen versucht, die Oberfläche des Polymers zu vergrößern.
Die so präparierten Polymerfilme wurden unter der Zuhilfenahme von spektroskopischer Ellipsometrie, Rasterkraftmikroskopie, Rasterelektronenmikroskopie und energiedispersiver Röntgenspektroskopie bezüglich ihrer Gleichmäßigkeit, der Topographie, dem Schwellverhalten und der chemische Zusammensetzung untersucht.
Die Resultate zeigen, dass ein pHEMA Polymerfilm ein ausreichendes Schwellverhalten besitzt, um mit spektroskopischer Ellipsometrie eine Änderungen der Dicke in Regionen niedriger Feuchtigkeit festzustellen. Die mögliche Verwendung als Material in Umgebungen mit niedriger Feuchtigkeit und als Material für einen Feuchtigkeitssensor in Erdgas ist damit gegeben. Es wurden mit Erfolg Nanoröhchen aus p(HEMA-co-EGDMA) unter Verwendung von anodisierten Aluminiumoxidmembranen als Formgeber hergestellt.

CONTENTS

LIST OF FIGURES

ACRONYMS

TEG Triethylene glycol

HEMA Hydroxyethyl methacrylate

MAA Methacrylic acid

TBPO Di-tert-butyl peroxide

CVD Chemical vapour deposition

iCVD Initiated chemical vapour deposition

SE Spectroscopic ellipsometry

EDX Energy dispersive x-ray spectroscopy

AFM Atomic force microscopy

SEM Scanning electron microscopy

ESEM Environmental scanning electron microscopy

1 INTRODUCTION

The Netz GmbH has to guarantee a safe and failure-free operating pipeline-system. What they want to achieve, is a minimization of corrosion and the formation of hydrate inside their pipelines, which means, that they also need to minimize the amount of water in the natural gas. In figure 1 the process of hydrate formation in an oil pipeline and pipe blockage is depicted, but this theory holds also for gas pipelines. Hydrates are formed in combination with CO_2 and O_2 due to the Joule-Thompson effect, either gas temperature change because of changes in pressure, due to different altitudes or changes in temperature because of aboveground components. The then formed hydrates tend to clog the pipes and the condensing water causes corrosion of the pipeline components. The goal of this master thesis is to

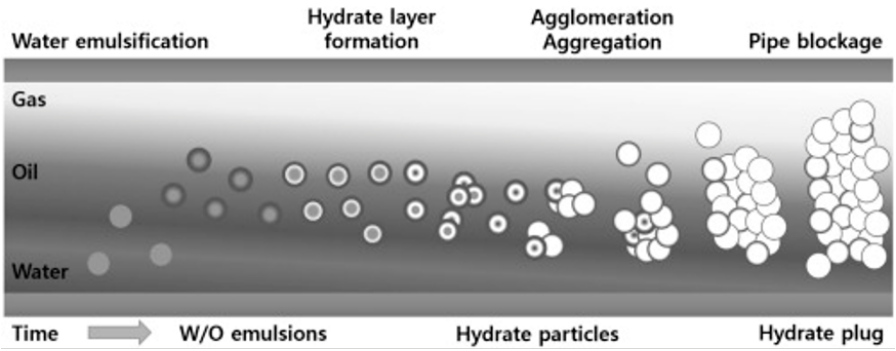

http://ars.els-cdn.com/content/image/1-s2.0-S0378381215301783-gr1.jpg

Figure 1: Schematic of hydrate formation in an oil pipeline. This also holds for gas pipelines. [2]

investigate, if polymer hydrogel thin films are responsive enough in low humidity regions, to use them as a material for a humidity sensor device and measure the relative humidity in a natural gas environment in pipeline systems. Hydrogels are stimuli-responsive polymer networks, which can absorb and retain water or water vapour due to their hydrophilic pedant functional groups, which means, that an increase of volume with the uptake of water can be observed. The humidity levels in natural gas in pipeline systems go down to the order of a few % relative humidity, which is a region where hydrogels are not widely used.
Initiated chemical vapour deposition is chosen as the method for synthesizing the polymer films. It is a versatile and powerful technology used for surface engineering, for applying polymer coatings without the use of a solvent. Because of its many advantages it is used in

biotechnology, nanotechnology, optoelectronics, photonics and sensing.
The first part of the thesis will deal with the fundamentals of polymers, CVD, the used chemicals, the experimental setup and the characterization techniques.
In the second part the different experiments which have been performed will be explained and the results discussed.

Part I

FUNDAMENTALS

This part covers the fundamentals and important information regarding humidity sensors, polymers and hydrogels as well as initiated chemical vapour deposition and its underlying concepts

2 HUMIDITY SENSORS

2.1 CONCEPT OF HUMIDITY

Humidity represents the amount of water vapour in a gaseous environment and it is an important factor when talking about many different areas. There are for example direct and indirect effects on our health, as we feel physical discomfort due to the fact that the relative humidity directly affects our perception of temperature. Also extremely low values will cause eye irritation and on the other hand higher values have shown to reduce the severity of asthma, helping with dry throats and nasal passages, and having an impact on the population growth and survival of infectious or allergenic organisms. [3] Electronic appliances may fail when the water content in the surrounding atmosphere is too high, so for properly operating appliances, such as high impedance electronic circuits, electrostatic sensitive components and high voltage devices it's important to know humidity values. As it is the motivation for this thesis, humidity also plays an important role when talking about physical effects that take place, for instance hydrate formation and oxidation in pipeline systems. There are different ways to specify the amount of water in the surrounding, often depending on the field of application. For the amount of water in a gaseous phase the terms absolute and relative humidity are commonly used. Absolute humidity is defined as the total mass of water m per the total volume of the wet gas V: $d_w = \frac{m}{V}$. Whereas relative humidity is defined via the ratio of the actual vapour pressure of the air at any temperature P_W to the maximum of saturation vapour pressure at the same temperature P_S: $RH = 100 * \frac{P_W}{P_S}$. [4] So the value of RH expresses the percentage of water vapour currently in a gas in regard to the maximal possible water vapour before it's saturated. Relative humidity values decrease with an increase in temperature since warm gases can hold more water vapour until there's saturation. One can calculate absolute humidity from known relative humidity and temperature.

2.2 TYPES OF HUMIDITY SENSORS

Instruments used for measuring humidity are called hygrometers and they have been investigated since as early as the 15th century. [5] The first mechanical hygrometers were often based on materials coming from animals or humans, like horse hairs or cat guts and their characteristics to contract and expand in response to the humidity. In general a material for a sensor has to be selective to water and has to have a property which changes with the concentration of water. Those kind of mechanical sensors have been used until the development and progression of the first electronic chips. Since then a wide range of humidity sensor types have emerged. In general they can be grouped into three major types of sensors, depending on the way to characterize them (fig. 2). In this work they will be differentiated on their basic approach to measure humidity, being either based on electronic, optical or acoustic effects. Electronic humidity sensors are based on the change of an electrical property, such as capacitance or resistance, whereas optical humidity sensors are based on interference effects and acoustic ones on resonance effects. Sensors based on the change of an electrical property, since they are under development for longer, especially capacitative ones, are the dominant technology, in terms of distribution, in industry at the time of writing. [4]

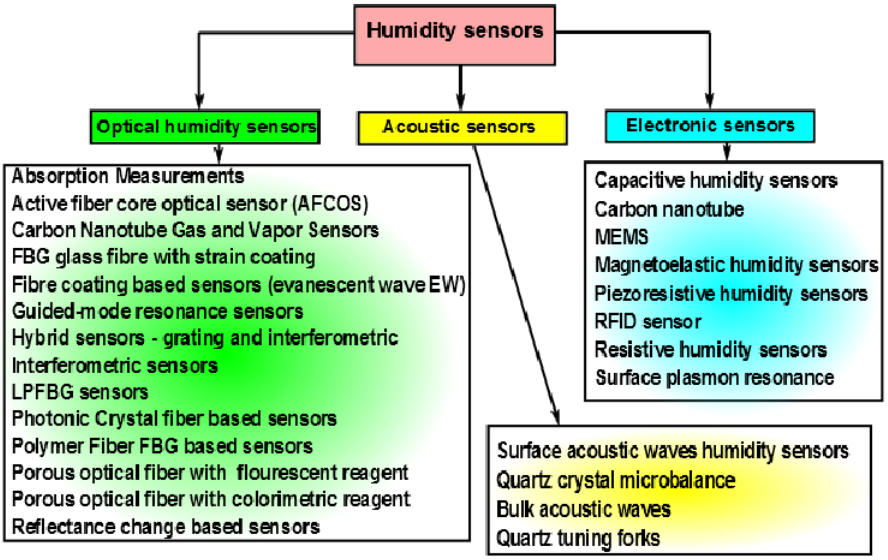

Figure 2: Different types of humidity sensors. [6]

2.2.1 *Electronic sensors*

The basic principle of electronic sensors is to measure a change in some electrical characteristic of a material sensitive to humidity. They can further be classified into conductive, resistive and capacitive sensors, based on the electrical property that changes and is measured. Advantages of this sensor type are that it can be produced fairly cheap, a sensor can already be bought for around 10 €, and their simple design. Electronic sensors are often built as breakout boards, integrating sensor elements plus signal processing on a tiny foot print and provide a fully calibrated digital output, ready for the use with a microprocessor. [7] But there are also some disadvantages: there is a need for regular calibration and a certain difficulty in measuring very low or high relative humidity levels. Also due to fact that electricity is needed for measurements the use in critical environments as for example in potentially explosive atmospheres like natural gas pipelines is either difficult or some times impossible. [8]

2.2.1.1 *Capacitive sensors*

The sensor being currently in use to measure the humidity inside the pipelines in natural gas is based on a HC1000 unit from E+E Elektronik, and the one used as a reference sensor for our measurements is a Sparkfun SHT15. Typewise both are capacitive polymer sensors, where a thin film of a suitable humidity sensitive material is deposited between closely spaced electrodes. These electrodes often have the form of two comb-like structures that are interdigitating. This increases the capacitance, allows the water vapor to interact with the surface of the thin film and is also easier to produce than structures with two electrodes on both sides. A schematic of such a structure can be seen in fig. 3.

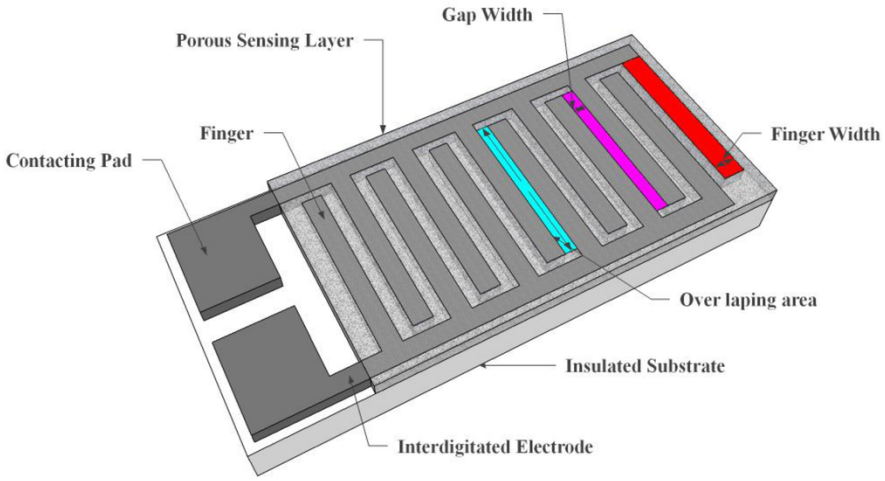

Figure 3: Schematic of a capacitive sensor element [4]

2.2.2 *Acoustic sensors*

The second type of sensors mentioned are acoustic ones, here the measurement is based on the change of some mechanical property of the humidity sensing material when water molecules are adsorbed on the surface. Figure 2 lists different methods of acoustic humidity measurement: Surface acoustic waves (SAW) and bulk acoustic waves (BAW) where absorbed water molecules lead to a change in the velocity of surface/bulk waves, the change in the resonance frequency of a quartz crystal microbalance (QCM) and quartz tuning forks (QTF). Due to the rise of water content, the density of the hydrophilic material changes and so does the resonance frequency, which can be detected.

2.2.3 *Optical sensors*

The third type are optical sensors, measuring the amount of water based on the change of optical constants of the sensing material. Some examples for different approaches to measure changes of those constants are spectroscopy, measuring changes in the reflectance [9], evanescent wave interactions [10], bragg and long period gratings [11], interferometers and interactions with photonic crystals [12]. The adsorbed water changes the optical properties of the sensing material, therefore a property of the light used gets modified and this is then detected. Optical sensors are a growing field of interest because they have specific advantages over other types of sensors, enabling the use in cases where electronic or acoustic ones are not suitable. Most of all, since they do not use electricity or the change of an electric property for measuring, they can be used in environments with electromagnetic fields or environments with inflammable gases. Optical sensors can be fabricated to have small dimensions and a small weight, making them useful in cases with space constraints [13].

2.2.3.1 *Dew point measurement - chilled mirror*

Most types of humidity sensors have problems in terms of repeatability, they show hysteresis, in other words the output of a sensor depends on whether the humidity is in- or decreasing. Typical values for hysteresis range from 0.5% to 1% RH [14]. This may not matter in many applications, but could also be a crucial and limiting factor, if precise humidity values are needed. An efficient, indirect method for humidity measurements with great precision is measuring the dew-point temperature. The dew point is the temperature to which air must be cooled down at constant pressure to become saturated with water vapour [15]. At this temperature the liquid and vapour phases are in equilibrium and if the air gets further cooled, there will be condensation. The approach to measure the dew point in an optical

hygrometer involves the use of a mirror, a LED light source and a light detector. The surface temperature of this mirror is precisely controlled by a thermoelectric heat pump. When air is floating over the mirror surface and the temperature of the surface crosses a dewpoint, water is condensing on the surface. The reflectivity of the mirror system changes due to scattering of light because of the water droplets. This change in reflectivity is detected by the LED light source - light detector system. Since the temperature of the mirror surface at the point when the reflectivity changes is the dew point, it is possible to calculate all moisture parameters like %RH, vapour pressure, etc. if the pressure is known. Precision is near 0.03°Celcius dew point and there is nearly no hysteresis. It is said to be the most fundamental and accurate method of measuring humidity but downsides are the relatively high cost, potential mirror contamination and the relatively hight power consumption by the heat pump. [14]

3

POLYMERS & HYDROGELS

3.1 POLYMERS

Polymers play a big role in our daily lifes, ones we often encounter are for example Polyethylene in form of cling film and plastic bags, Polyester in form of PET plastic bottles or polymethylmethacrylate in form of plexiglas.
According to the IUPAC (The International Union of Pure and Applied Chemistry) a polymer (from the ancient greek word "polumeres" meaning "consisting of many parts") is a substance composed of macromolecules. A macromolecule itself is a molecule with a high relative molecular mass and is in turn formed by the repetition of smaller units, called monomers (from greek meaning "single part"). The monomers, with a relatively low molecular mass, are covalently bonded to each other providing the so called backbone of a polymer forming long, chain-like molecules elongated in one direction in the most simple case. The possibility of the single, covalently bonded monomer units to rotate around the bonding axis leads to a high number of internal degrees of freedom and furthermore to a high number of possible spatial arrangements. Since carbon atoms, which have a high molecular mass, are the main component of the organic backbone of polymers, specific properties like viscoelasticity or toughness can be observed. Polymer chains do not have to be only linear, but can also be branched or even cross-linked as indicated in fig. 4 (a)-(e). [16]
One can distinguish between two types of polymers. If a polymer consists only of one monomer, it is labeled as a homopolymer (like polyethylene, fig. 5 or polystyrene, fig. 6), but polymers can also be composed of different monomers, leading to copolymers like acrylonitrile butadiene styrene (ABS) (fig. 7).
The process of forming a polymer out of monomers is called polymerization. There are different types of polymerization, but the one important in initiated chemical vapour deposition is radical polymerization, where polymers are created in a radical chain reaction pattern. The reaction is initiated via radicals, which are created by exposure to high temperature and which are normally provided by initiators, molecules that have a labile bond that can be broken creating radicals. As a next step those radicals bond with the monomers creating modified monomer-radicals growing to a polymerchain as more and more monomers attach.

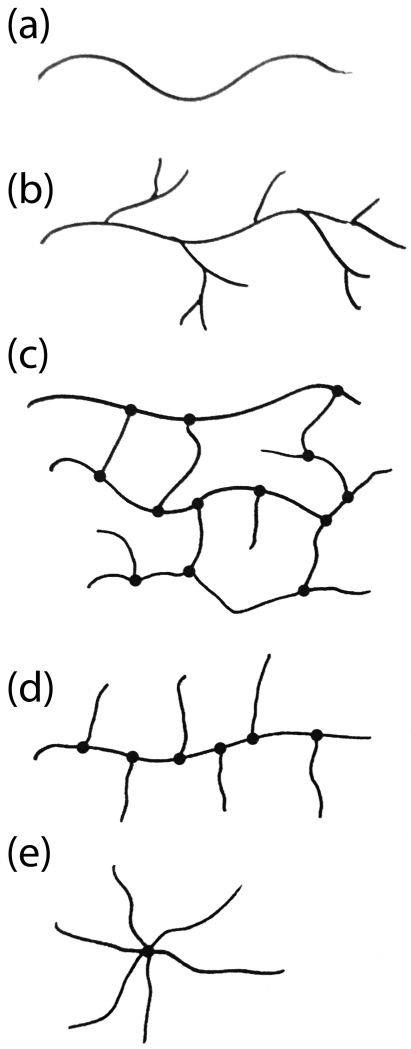

Figure 4: Possibilities of linking polymers. [16]

3.1.1 *Copolymerization*

If two monomers are involved in the polymerization process, one can identify different modes of copolymer growth, depending if the monomers grow in an regularly alternating fashion (A-B-A-B, 12 b), in blocks (A-A-A-B-B-B,12 c), or completely random (A-B-B-A-B-A-A,12 a) when there is no pattern recognizable. In iCVD, two types of copolymerization have been observed, namely alternating copolymerization and random copolymerization, where a study of reactivity ratios indicates that random copolymerization is more common [20]. Co-polymerization is an easy way to include desired properties and structural components into a polymer thin film synthesized by initiated chemical vapour deposition. This method enables synthesizing copolymers that would show miscibility issues, bypassing the downsides of solution phase synthesis, while also keeping the pedant functional groups intact, resulting in a polymer with a well-designed

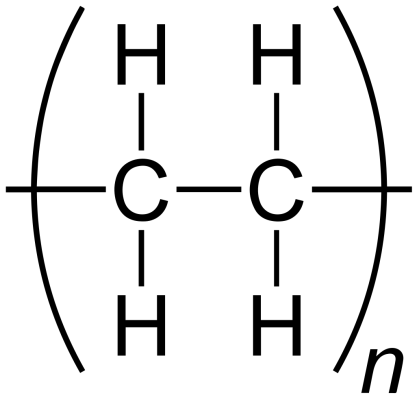

Figure 5: Chemical structure of polyethylene. [17]

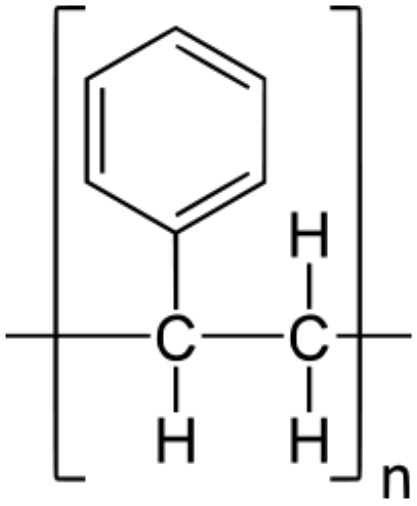

Figure 6: Chemical structure of polystyrene. [18]

structure. [21] As explained in chapter 4, iCVD also provides the capability to optimize and control the thin film properties by varying the flow ratios of the different monomers during the process of thin film formation. This is possible since the polymerization kinetics depend on the concentrations of the monomers and their respective reactivity ratios, so monomers with higher reactivity ratios will be more present in the resulting thin film.

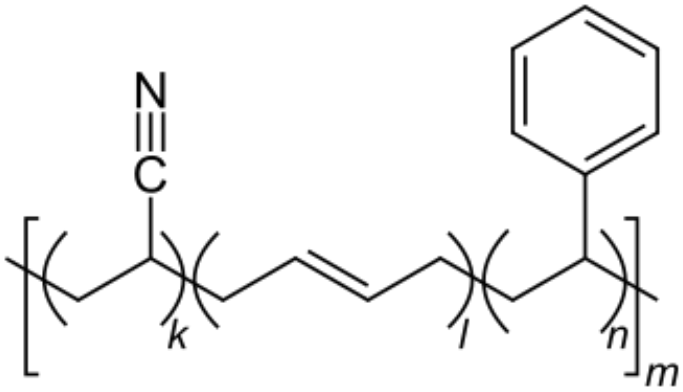

Figure 7: Chemical structure of ABS. [19]

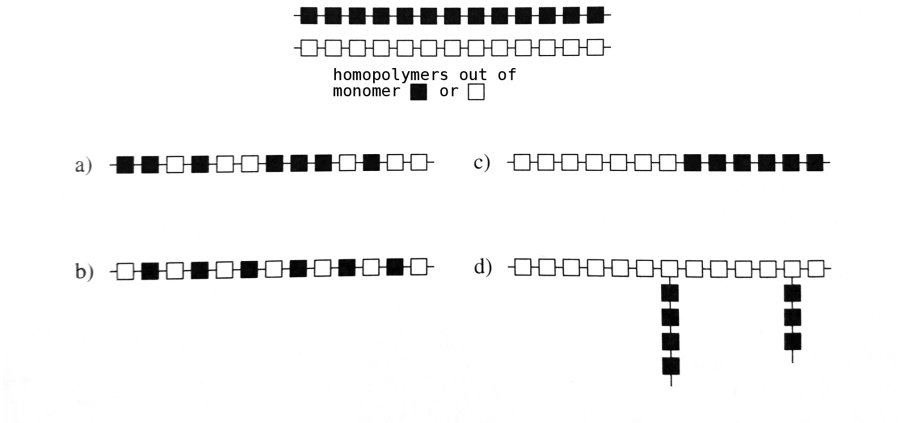

Figure 8: Possibilities of (co-)polymeric growth. [20]

3.2 CROSSLINKING

Another way to tune polymer properties is cross-linking. By incorporating a so-called cross-linker, the mechanical properties, such as youngs modulus or toughness, of a (co-)polymer can be altered. A cross-linker is a molecule, that links two polymer chains by creating a bond between them, forming a bridge. An example is rubber (fig. 9), natural rubber is runny at high temperatures and brittle when it's cold, but when links are created, by using sulfur to tie the seperate polyisoprene chains to one another, the rubber will not melt anymore but also will not break that easily when cooled. [22] In figure 10 the schematic of such cross-links is shown for the mainly used polymer in this work.

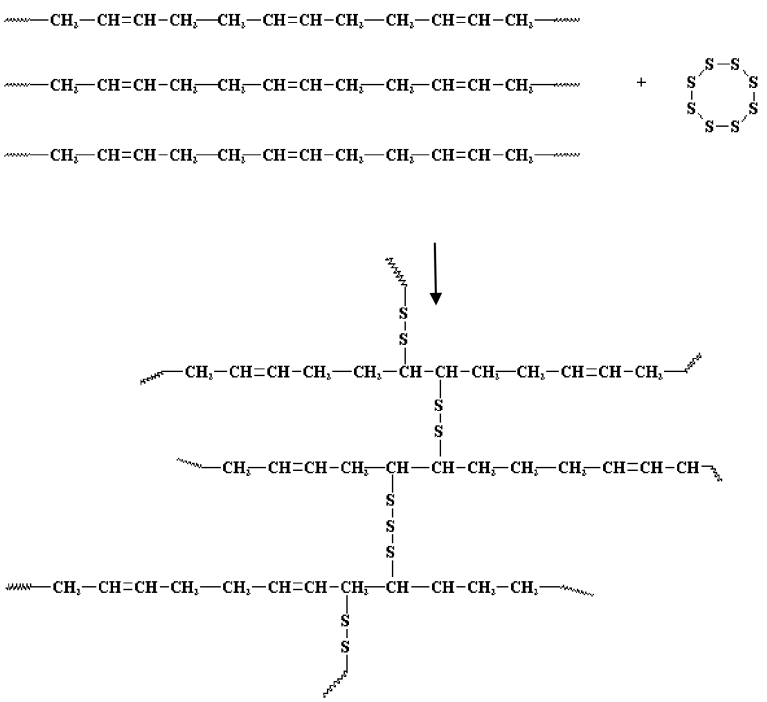

Figure 9: The figure shows how the cross-linker sulfur holds the separate polyisoprene chains together. [23]

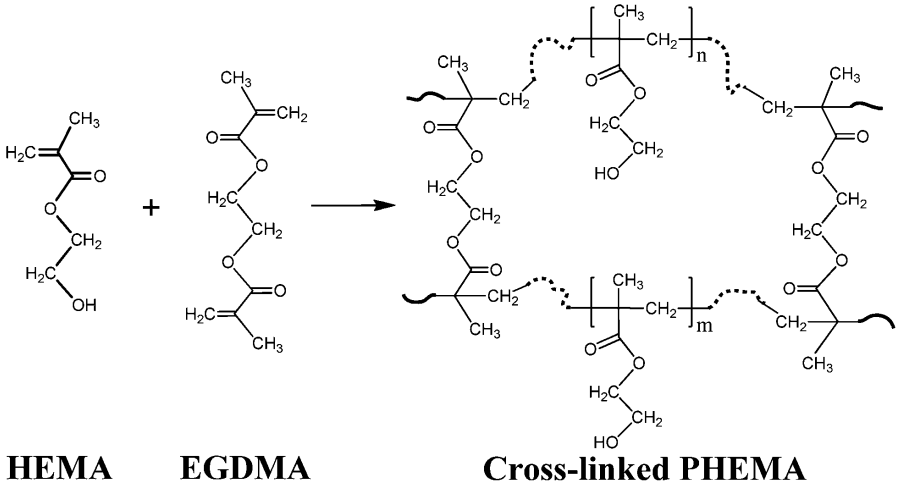

Figure 10: The cross-linker EGDMA holds the separate HEMA monomer molecules together, forming the cross-linked polymer p(HEMA-co-EGDMA)(right). [23]

3.3 HYDROGELS

In general hydrogels are water-unsolvable polymer networks, which can absorb and retain water (vapor) due to their hydrophilic pedant functional groups, which means, that they increase their volume with the uptake of water. This so called swelling can be measured with different techniques (see also 2) and calculated back to get a humidity value. As already mentioned, introducing a cross-linker changes the mechanical properties and normally one would use a cross-linker with hydrogels to guarantee their stability in water, but in a humid environment, especially with low levels of humidity, cross-linking is not required. Since the degree of cross-linking determines the mesh size (the average distance between two cross links) and the mechanical properties, it also affects the ability to swell in water. With an increase of the cross-linker ratio, there are more bridges between the individual polymer chains and the ability to swell decreases (see fig. 11).

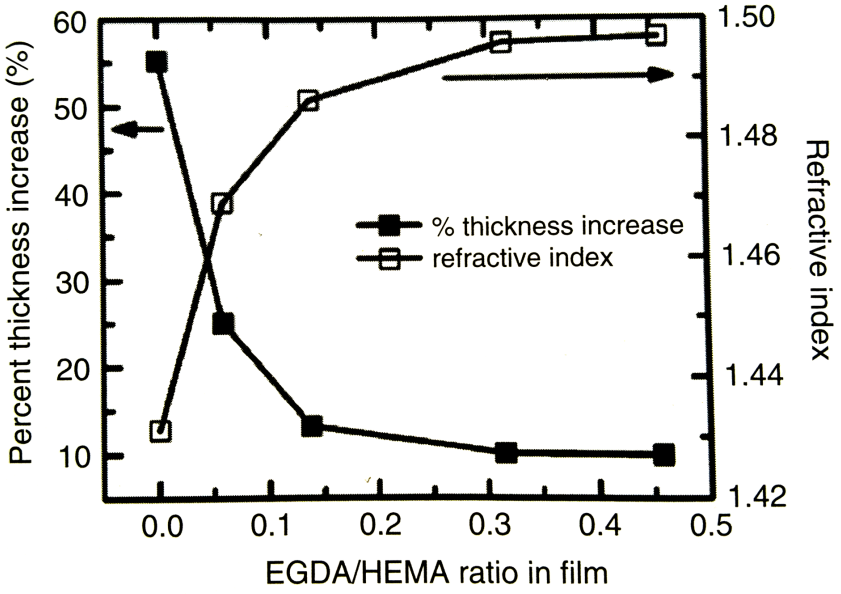

Figure 11: Changes in film thickness and refractive index of swollen film as cuntions of the EGDMA/HEMA ratio in the film. [21]

4 INITIATED CHEMICAL VAPOR DEPOSITION

4.1 CHEMICAL VAPOUR DEPOSITION

Chemical Vapour deposition is a versatile and powerful technology used in surface engineering, for depositing polymer coatings without the use of a solvent. Because of its many advantages it is used in biotechnology, nanotechnology, optoelectronic, photonics and sensing. It is a technique where vapours of volatile monomers are directly converted to form a solid macromolecular film on a substrate. Since there is no need to dissolve the macromolecules beforehand the synthesis of insoluble polymers, highly cross-linked organic networks and the polymerization of monomers not working with solution based processes is possible, while still achieving low impurity levels. [21] Due to its high conformality and low substrate temperature during the process it is applicable on nearly every substrate surface, even on fragile substrates like tissue paper or porous polymer membranes. Layered or even graded polymer compositions can be easily obtained by simply changing the ratio of used monomer gases introduced into the CVD reactor. This, in combination with a preservation of the organic functional groups, enables a precise and systematic control over the thin film properties, by simply choosing the appropriate monomers. Every CVD process consists of the same basic series of chemical and physical steps to form a polymer film:

1. Diffusion of the reactants through the gas phase to the reaction zone
2. Creation of new reactive species through a chemical reaction in the gas phase
3. Transport of the reactants and products to the substrate surface
4. Adsorption on the surface
5. Chemical reaction leading to polymerization at the surface and therefore film growth

This series of basic steps is also depicted in fig. 12. [21]

4.1.1 *Conformality*

The ability to conformally coat even complex three dimensional structures is one of the features distinguishing iCVD from other techniques. Conformal films can only grow when reactants in vapour

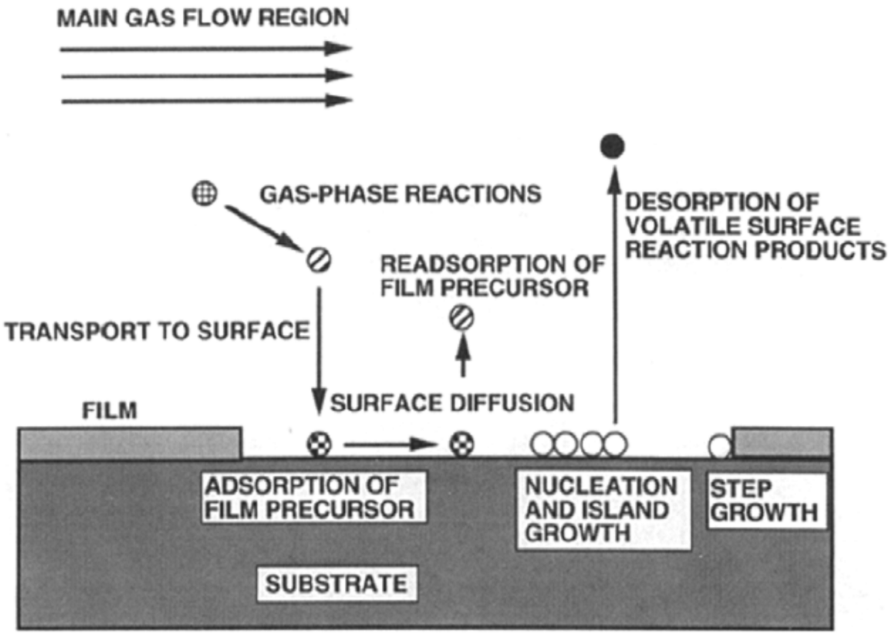

Figure 12: Schematic of the basic steps of a CVD process. [21]

phase are able to diffuse into small geometries like trenches and pores before they are bound. Now there are two mechanisms for surface reactions to take place, namely the Langmuir-Hinshelwood mechanism, where the two reacting molecules are both surface-bound and the Eley-Rideal mechanism, where a molecule from the gas phase collides with a surface-bound molecule and reacts. Figure 13 shows a drawing of the two mechanisms. Since the time scale for a reaction of a molecule colliding with a surface-bound one and being irreversibly bonded is a factor of 10 longer than the surface lifetime of an adsorbed reactant, the Eley-Rideal mechanism is the favoured mechanism. Diffusion into small geometries, enabling the conformal coating, is only possible if the probability that an impinging molecule chemisorbs on the surface is lower than the rate of diffusion. This probability is the so called "sticking coefficient" or "sticking probability". [21] If the concentration of the initiator radicals is high enough the reaction kinetics and therefore the sticking probability, but also the growth rate depends on the monomer surface coverage. This is, because the higher the coverage, the higher the probability that an impinging radical hits one of the monomer molecules on the surface and reacts with it. The monomer surface coverage in turn mostly depends on the monomer saturation ratio S, between the monomer partial pressure (P_m) and the saturation pressure at the substrate temperature (P_sat). A visual comparison of the conformality for different $\frac{P_M}{P_{sat}}$ values is shown in fig. 14.

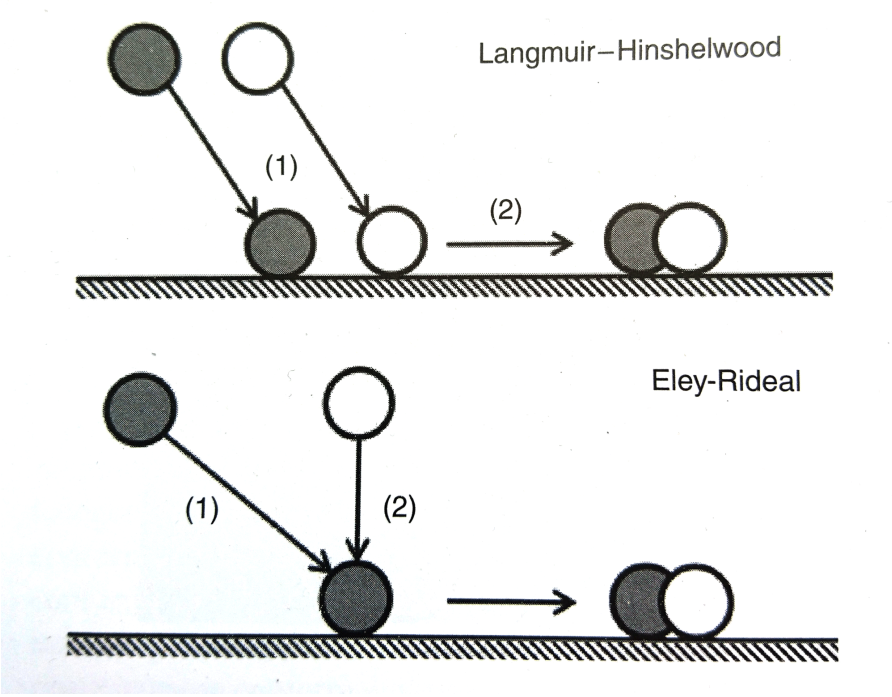

Figure 13: Drawing of the Langmuir-Hinshelwood mechanism (top) and the Eley-Rideal mechanism (bottom). [21]

4.1.2 *iCVD*

In an iCVD, or CVD, process all reactants are introduced as vapours into the vacuum chamber of the reactor. The combined line for connecting the monomers to the chamber and their jars are heated to prevent adsorption in those lines and assist the evaporation. To avoid breaking the labile O-O bond, the initiator and it's separate line to the vacuum chamber are not heated. The flow rates of the reactants can be regulated separately for every reactant with needle valves. As already mentioned in chapter 3 the important polymerization type in initiated chemical vapour deposition is radical polymerization. For this, as a first step, the monomers (M) and the initiator (I) are introduced into the vacuum chamber through their respective lines. The monomer units then adsorb on the back-cooled stage and the initiator molecules come into contact with resistively heated filament wires, suspended a few centimeters above the substrate. The initiator has a labile O-O bond, and already breaks down into radicals (R) when exposed to relatively low temperatures of about 200-250deg C. This decomposition is selective, which means, that only the initiator molecules are affected, leaving the monomers intact, since the temperature needed for decomposing would be over 500deg C. The resulting radical fragments only react with the vinyl bonds of the monomers adsorbed on the cooled surface, creating modified monomer-radicals, beginning the polymerization and growing to a polymerchain (P) as

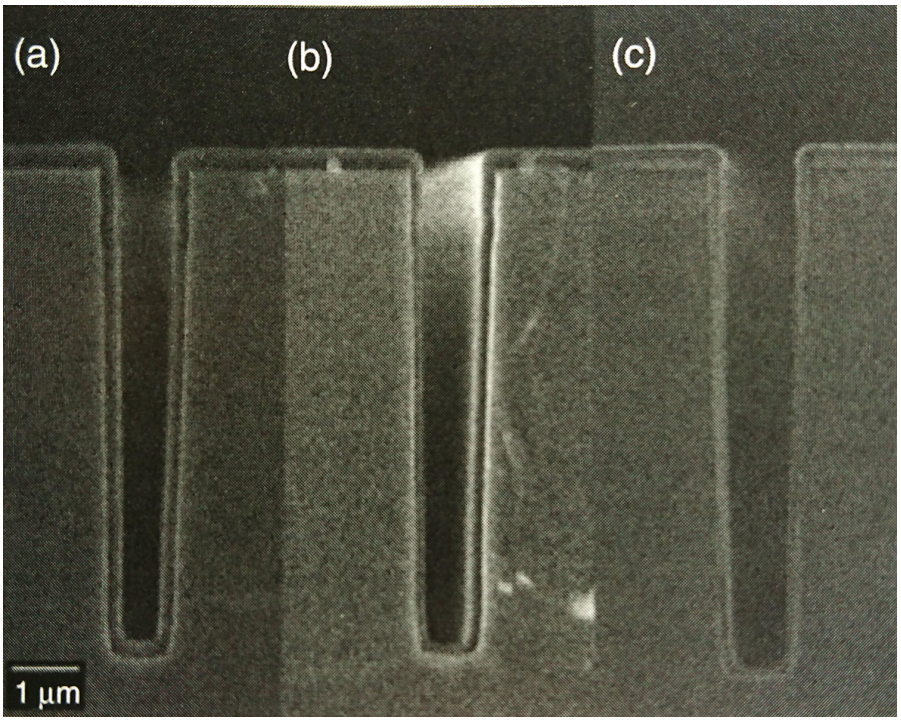

Figure 14: Comparison of deposited films in trench structures. Because $\frac{P_M}{P_{sat}}$ increases from (a) to (c), the confomality decreases [21]

more and more monomers attach. The schematic of this series of steps is depicted in fig. 15. The initiator mainly used in iCVD and in

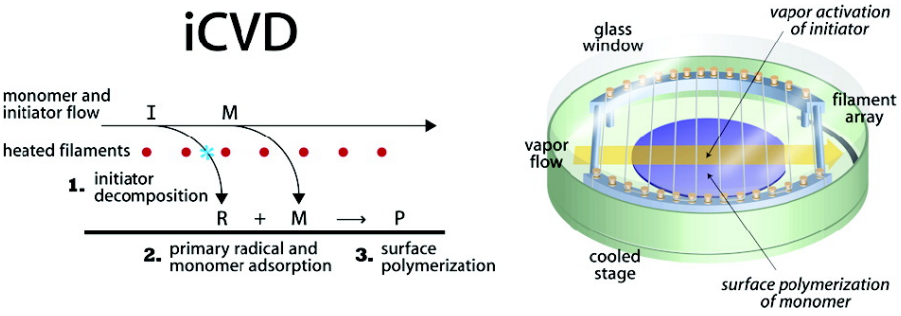

Figure 15: Schematic of the basic steps of an iCVD process inside a reactor. [24]

this work is di-tert-butyl peroxide and is shown in fig. 18. In addition to the advantage of preserving the functional groups, which is essential for synthesizing polymers sensitive to external stimuli, the low substrate temperature allows the use of fragile substrates like tissue paper or contact lenses and since it is not a line of sight technique, it provides the application on complex three dimensional structures, depositing highly conformal thin films. How conformal the deposited films are in comparison to other techniques can be seen in fig. 17.

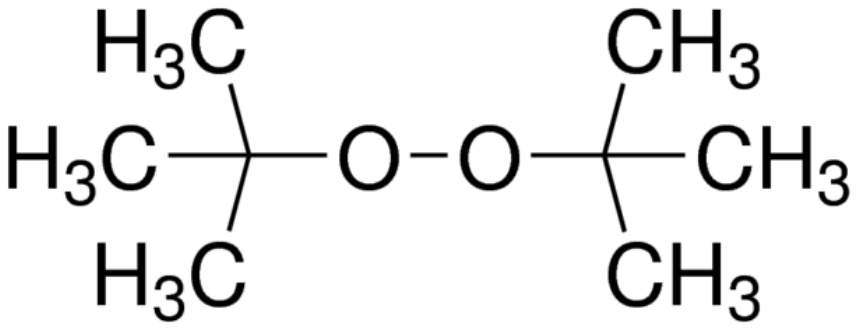

Figure 16: Structural formula of TBPO. [25]

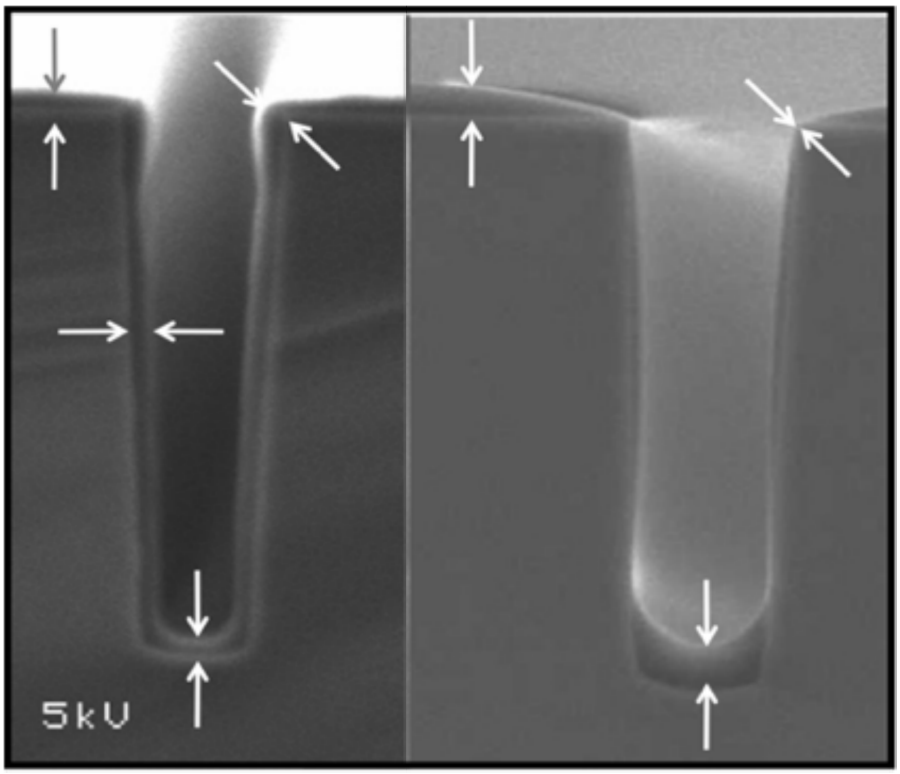

Figure 17: Comparison of a polymer coating in trench structures, from left to right between iCVD, spincoating and plasma polymerization. [21]

5 CHEMICALS

The following chemicals were used in this work for the synthesis of polymer thin films in different combinations.

5.1 INITIATOR

As an initiator tert-Butyl peroxide (TBPO, 98% , Sigma Aldrich) was used. It's chemical structure is depicted in fig. 18. It has a labile oxygen-oxygen bond, which can be broken by supplying energy equivalent to temperatures above or around 200deg C creating radicals needed for initiating the iCVD process.

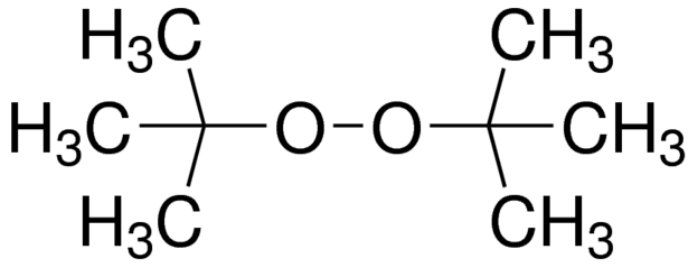

Figure 18: Chemical structure of tert-Butyl peroxide (TBPO). [25]

5.2 CROSS-LINKER

As a cross-linker ethylene glycol dimethacrylate (EGDMA, 98%, Sigma Aldrich) was used. It's chemical structure is depicted in fig. 19. EGDMA is used as a cross-linker to enhance the mechanical stability of a polymer film, especially when high humidity values could lead to dissolution. An example of the cross-linked polymer p(HEMA-co-EGDMA) is shown in fig. 10.

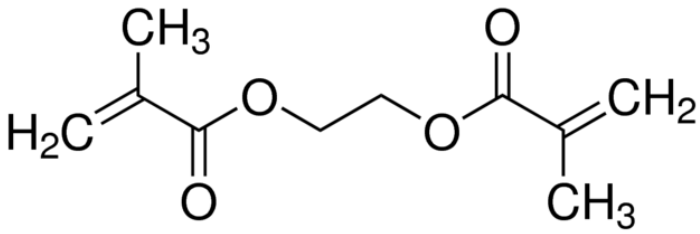

Figure 19: Chemical structure of ethylene glycol dimethacrylate (EGDMA). [26]

5.3 MONOMERS

5.3.1 *HEMA*

2-Hydroxyethyl methacrylate (HEMA, 97%, Sigma Aldrich) was used as the main monomer because of it's hydrophilic nature. It's chemical structure is depicted in fig. 20. HEMA is hydrophilic due to its O and OH groups.

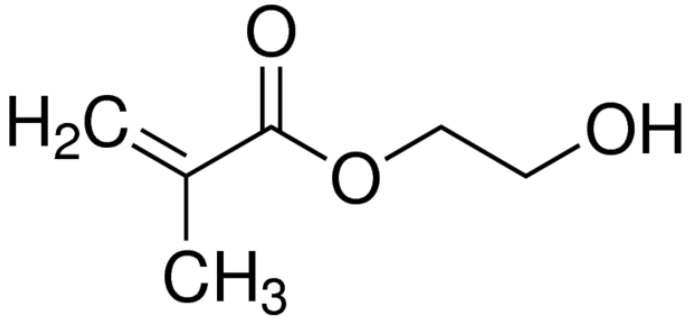

Figure 20: Chemical structure of 2-Hydroxyethyl methacrylate (HEMA). [27]

5.3.2 *MAA*

To enhance the hydrophilicity of the polymer films methacrylic acid (MAA, 99%, Sigma Aldrich) was used. It's chemical strucuture is depicted in fig. 21.

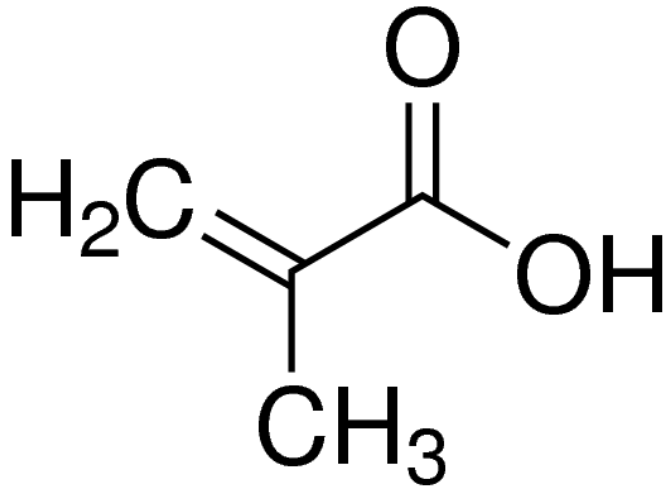

Figure 21: Chemical structure of methacrylic acid (MAA). [28]

6 ICVD SETUP

6.1 SAMPLE PREPARATION

In this work two different types of films were produced, namely planar thin films on silicon substrates and nano structured tube forests on anodized aluminium oxides. Since the anodized aluminium oxides membranes (Anodisc 25, Whatman) used as templates for the nano structured films are very brittle, no cleaning was done. For the planar thin films silicon wafers (Siegert Wafer) were used as substrates for deposition, since they allowed the use of spectroscopic ellipsometry as an optical measurement technique. Those wafers can be cut into pieces of needed size using a diamond tip scriber. The pieces were then cleaned with isopropyl and a lint free paper wipe to ensure a clean surface and therefore get more homogeneous polymer films. The samples were than put into the vacuum chamber of the iCVD reactor.

6.2 DEPOSITION PROCESS

This section will give a general description of the used equipment and the steps necessary for the deposition process. The iCVD reactor is a custom built reactor setup as it is depicted in fig. 22. Since there are processes involved that need a long time to get into equilibrium there is some preparation done before the actual deposition process. After placing the samples for the deposition and an additional piece of silicon wafer, which is used for the in-situ growth control, on the bottom of the vacuum chamber, it is closed and the line connecting the roughening pump (PFEIFFER VACUUM DUO 65) to the chamber is opened to create a base pressure in the range of 1 mTorr. The temperature of the stage and the substrate can be controlled by a chiller (THERMO SCIENTIFIC ACCEL 500LC). The monomers used for the iCVD process in this work are all liquid and need to be heated to promote evaporation and to ensure a gas flow of the monomers into the vacuum chamber. Since premature decomposition is not desired, the initiator has its own line leading into the chamber, which is not heated. The heating of the monomers and the controller for the stage temperature needs to be turned on long enough before the deposition to ensure that a thermodynamic equilibrium is reached. This is done by turning on and setting the right temperature on the respective heating control units (OMEGA MCS-2110K-R) for every monomer used. To have in-situ monitoring of the

film thickness, laser-interferometry is used. For this a cleaned piece of a silicon wafer was put into the vacuum chamber and the beam of a He-Ne laser (THORLABS HNLS008L-EC) pointed onto it. Again, to reach an equilibrium state, the laser needs to be turned on long enough before. When the equilibrium of the system is reached, the next step is to check the leak rate of the system. This is done by using a LabView program, which acts as a graphical user interface for operating the pressure controller (MKS 600 series pressure controller 651CD2S1N). This controller drives an adjustable valve that connects the vacuum chamber and the roughening pump. The leak rate was calculated automatically in the LabView program by recording the pressure increase over time when the aforementioned valve is closed. As a next step the flow rates of the monomers, the initiator and nitrogen, if used to bias the saturation ratio, are adjusted separately, in order of how volatile they are. For this, only the needle valve connecting the respective jar to the line leading to the vacuum chamber is opened and again automatically the valve connecting the roughening pump is closed, the pressure increase recorded and a flow rate in standard cubic centimeter per minute (sscm) calculated by the LabView program. This is an iterative process, the needle valves need to be adjusted if the flow rate is too high or not high enough. For nitrogen a separate mass flow controller (MASS FLOW CONTROLLER) is used, where a fixed flow rate in sscm can be set. After the flow rates have been set, all lines are opened and a constant working pressure in the range of 200 to 350 mTorr, depending on the deposition parameters, is set on the pressure controller. When the working pressure is reached, the power supply (HEINZINGER PTN 350-5) for heating the filament wires to a temperature of about 250deg can be turned on to start the iCVD process by decomposing the initiator molecules. During the deposition the intensity of the reflected laser beam is measured and recorded as a function of time. One oscillation of the intensity corresponds to roughly 200 nm of applied polymer film (fig. 23). When the desired film thickness is reached, the process is ended by closing the monomer valves, after three more minutes closing the initiator valves (to cap the dangling bonds) and then turning of the filament heating and the nitrogen flow.

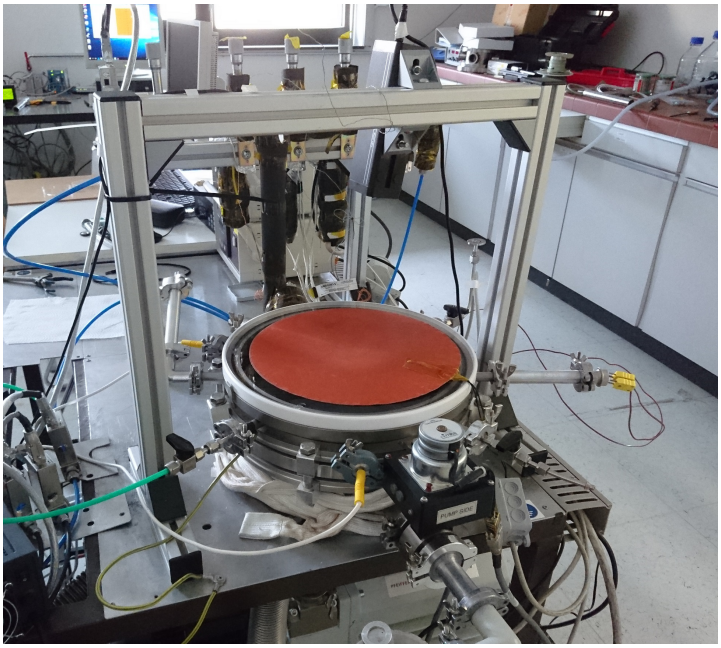

Figure 22: Picture of the custom built iCVD reactor setup.

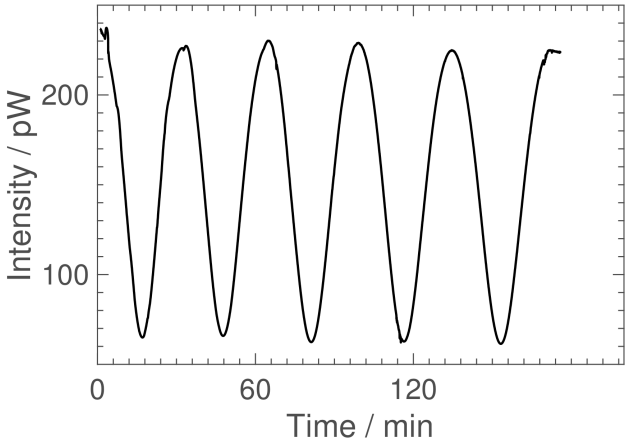

Figure 23: Recorded data from in-situ laser-interferometry to monitor film growth. One oscillation of the intensity corresponds to roughly 200 nm of applied polymer film. [29]

7

SPECTROSCOPIC ELLIPSOMETRY

For the actual in-house measurement of thickness change a J.A. Woollam M-200 was used for spectroscopic ellipsometry on. Ellipsometry is an optical measurement technique that measures the change in polarization as light gets reflected off of a sample surface. This is also what it's named after, since linearly polarized light is often elliptically polarized after reflection. Ellipsometry offers advantages like a high precision, on a sub angstrom level, it is non-destructive and there's the possibility of real-time monitoring. [30]

7.1 UNDERLYING CONCEPT

Two values (ψ , Δ), representing the amplitude ratio (ψ) and the phase shift (Δ) between the p- & s-polarized components of the reflected light beam are measured, from those values optical constants and the film thickness can be deduced. Figure 24 shows an illustration of the measurement principle, where the incident light beam on the left is linearly polarized and the reflected beam is elliptically polarized after interacting with the sample surface. For simple sample structures the

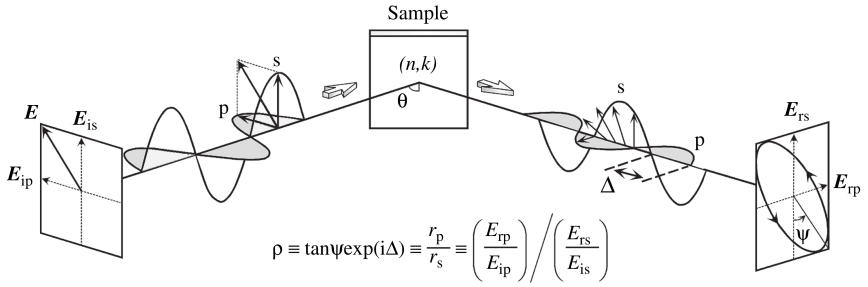

Figure 24: Illustration of the measurement principle of ellipsometry. [30]

refractive index n and the extinction coefficient k can be measured directly, since the amplitude ratio ψ is characterized by the refractive index n and the phase difference Δ by the absorption coefficient k. With n and k the complex refractive index $N = n - ik$ can be calculated and from there the complex dielectric constant $\epsilon = N^2$ or the absorption coefficient $\alpha = 4\pi * \frac{k}{\lambda}$ can be obtained. [30]
The measured values for ψ and Δ are defined by ratio of the amplitudes of the p- and s-polarized reflected beams:

$$\rho(N_0, N_1, N_2, d, \Theta_0) = \tan(\psi) * e^{i\Delta} = \frac{r_p}{r_s} \tag{1}$$

With the ψ the amplitude ratio, Δ the phase difference, r_p the amplitude of the p-polarized component of the reflected beam and r_s the amplitude of the s-polarized component of the reflected beam. N_0, N_1, N_2, d and Θ_0 denote the complex refractive indices of air, the thin film and the substrate, the thin film thickness and the incident angle respectively, as shown in fig. 25. To get ψ and Δ spectra the

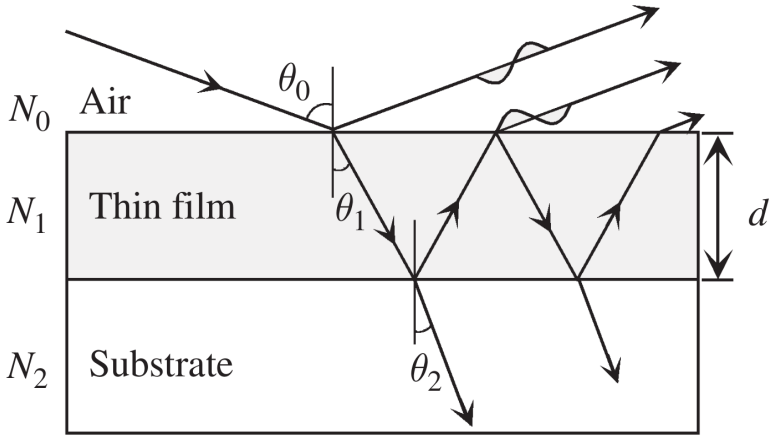

Figure 25: Illustration of the optical model of an air/thinfilm and thinfilm/-substrate structure. [30]

wavelength of the incident beam is varied, usually in the ultraviolet or infrared range. Since the p- and s-polarized components can't be distinguished at a normal incident angle, measurements are done at oblique angles.
A materials optical constants will vary for different wavelengths, for further analysis they must be described by a model at all wavelengths probed with the ellipsometer. The dispersion relationship used as a model for data analysis in the experimental part is the Cauchy model:

$$n(\lambda) = A + \frac{B}{\lambda^2} + \frac{C}{\lambda^4} \tag{2}$$

It is an empirical relationship between the refractive index n and the probing wavelength λ. To calculate the refractive index the parameters A, B and C are fitted to best reproduce the curve obtained from the measurement, as it is shown in fig. 26. For in-situ determination of the film thickness in the experimental part an enclosed temperature controlled stage (THMS350V) was used, since it provides the ability to flow in gases with different levels of humidity. Figure 27 shows the ellipsometer with the enclosed stage mounted. With this stage a three angle measurement cannot be performed, instead the acquisition is performed at an angle of 75deg in a wavelength range from 370 to 1000 nm. The stage has also a built in element for heating

and cooling, therefore temperature ramps can be applied during measurements. In the CompleteEASE Software (J.A.Woollam) a model consisting of a silicon substrate, a 1.7 mm SiO_2 layer on top and a Cauchy layer representing the transparent polymer film is used to fit the data (fig. 28).

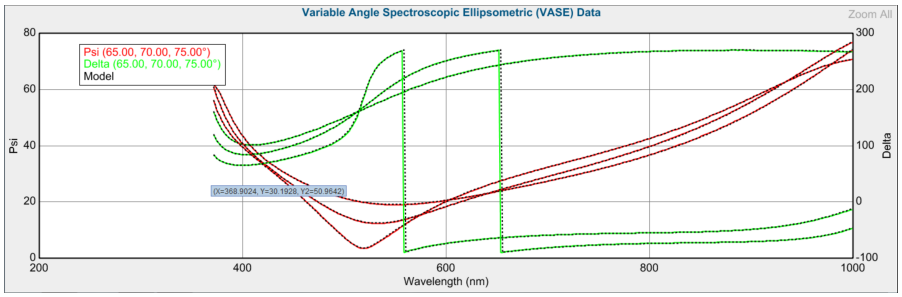

Figure 26: Variable angle spectroscopic ellipsometric data for Ψ and Δ for three angles, where a Cauchy model was used to fit the data (black dotted line).

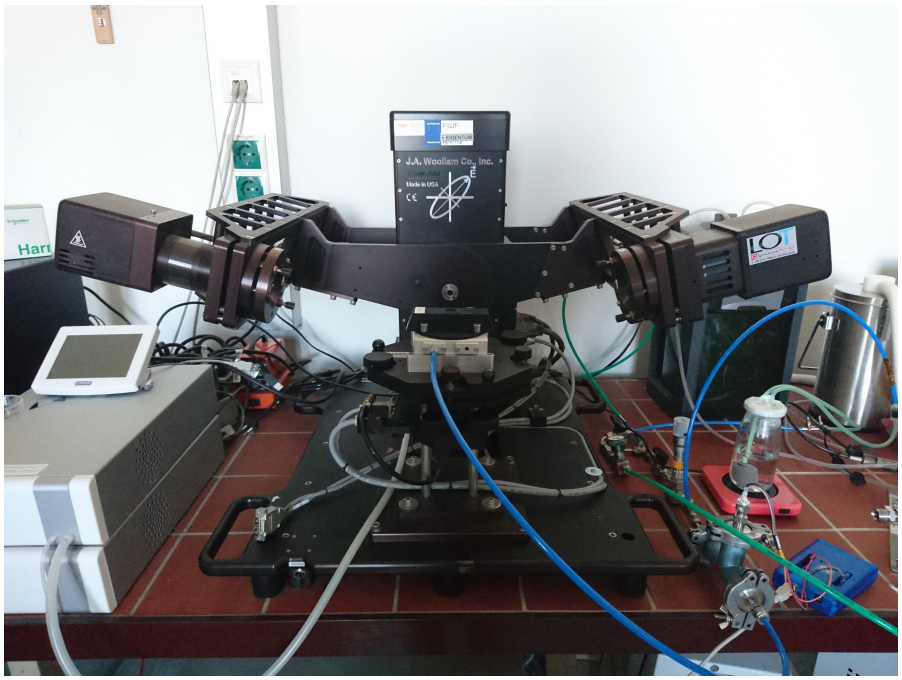

Figure 27: Ellipsometer with the enclosed temperature controlled stage THMS350V mounted.

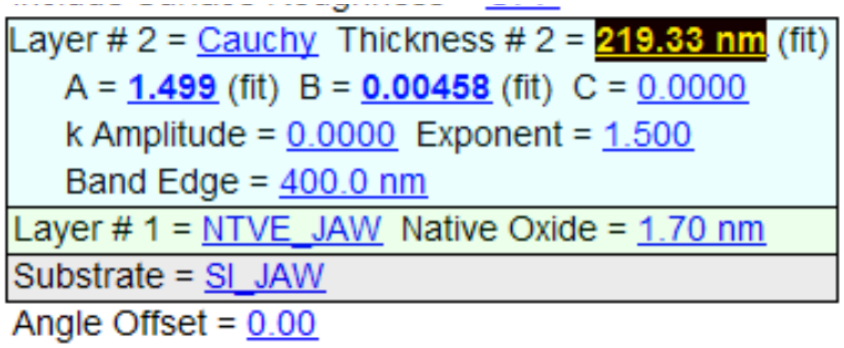

Figure 28: Screenshot of the Cauchy model used in the CompleteEASE software provided by J.A. Woollam. The optical constants A and B as well as the film thickness of the Cauchy layer were fitted.

8 HUMIDITY SETUP

8.1 ELLIPSOMETER STAGE

As already mentioned in chapter 7, an enclosed stage (THMS350V, fig. 29) was used with the ellipsometer to be able to measure the change of thickness of the synthesized polymer films at different humidity values. This provides the possibility of in-situ ellipsometry measurements, being able to adjust humidity and measure the polymer films thickness during the swelling experiments. The stage has

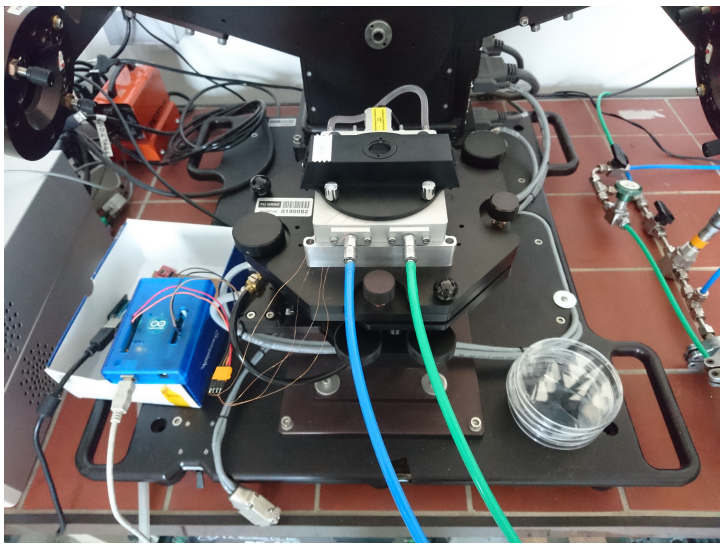

Figure 29: THMS350V, enclosed stage for the ellipsometer.

in- and outlets to be able to flow in gases, a heating stage, and there is enough space to fit the reference humidity sensor inside. Using the ellipsometer software CompleteEASE and the described setup, it is possible to do measurements at different stage temperatures and also include temperature ramps to heat or cool the sample stage during measurements.

8.2 CUSTOM MIXING CHAMBER

To gain the ability to adjust the humidity of a gas mixture during a measurement inside the enclosed stage, a custom external mixing setup was built (30). This external setup is connected to the aforementioned in- and outlets via tubes and provides the capability to mix "dry" inert gases (with approx. 3 ppm of H_2O molecules) with humidified inert gases, coming from a bubbler, and natural gas being

supplied by sample cylinders.

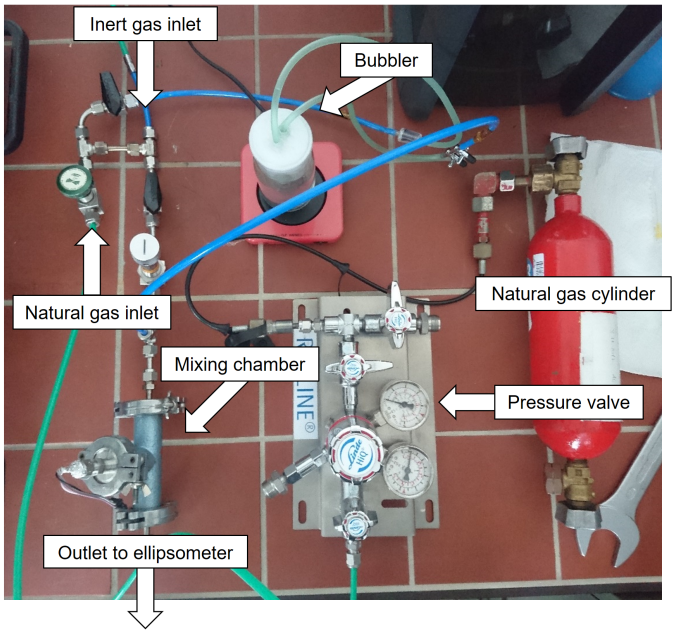

Figure 30: Custom humidity mixing setup.

On the top of figure. 30 there is an inlet for the inert gases. The line is then split up, a part of the flow going to the bubbler and getting then fed back to the main line. The flow to the bubbler can be adjusted by valves. The bubbler itself can be heated from the bottom with a cup warmer, if very high humidity values of above 90 % relative humidity are necessary. On the very right, a sample cylinder for natural gas is connected. Those cylinders have their own pressure valve, the outlet from this valve leads to a valve on the left, back to the main line. In the lower left corner of the picture you can see a chamber, to let the gases mix better and also to be able to insert another humidity sensor, if needed. With this setup it is possible reach humidity levels from nearly 0 % (value of the used inert gas) to 100 % RH in 1 % steps so far.

9 FURTHER ANALYSIS TECHNIQUES

9.1 ATOMIC FORCE MICROSCOPY

Atomic force microscopy is used in the experimental part for morphological analysis of the anodized aluminium oxide membranes and is tried as a technique for analysing the swelling of a single nano tube of the nano-structured polymer films. The morphological analysis of the AAO membranes was done in-house on a Nanosurf EasyScan2, while the swelling experiment took place at the Montanuniversität Leoben, where they have an AFM with an Olympus AC160TS cantilever with a tip radius of about 10 nm and a humidity chamber built around the AFM, in collaboration with Prof. Christian Teichert.
Atomic force microscopy is a scanning microscopy technique where a cantilever with a very sharp tip is guided over the sample surface linewise with the use piezoelectric elements. Attractive and repulsive forces cause the cantilever to deflect towards and away from the sample surface. A laser beam is pointed onto the cantilever and is reflected onto a segmented photodetector, which detects the cantilever movements. This is the reason why an AFM is normally mounted on an attenuation table to compensate for small oscillations or interferences. A schematic of an atomic force microscope is shown in figure 51. The measurements in this thesis are all performed in non-contact mode where the cantilever is driven so that it oscillates. The force interactions between the sample surface and the cantilever are measured when approaching by measuring the change in resonant frequency directly. Using a loop-back circuit to always drive the sensor on it's resonance frequency the distance between the tip and the surface is adjusted, giving a topographic image of the sample. In the AFM Software parameters like the free vibration amplitude, the setpoint, and have to be changed for every sample in a PID-controller-like fashion to get good results. The software package Gwyddion can afterwards be used to digitally process the recorded pictures.

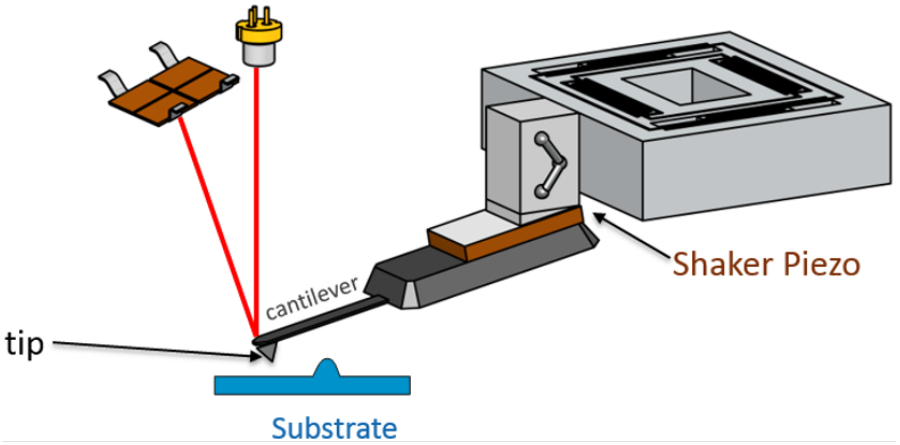

Figure 31: Schematic of an atomic force microscope. [31]

9.2 SCANNING ELECTRON MICROSCOPY

A scanning electron microscope (SEM) uses a focused beam of electrons to scan a sample surface. All SEM's have the same basic setup, containing an electron column, where an electron gun generates the electron beam, a sample chamber, various detectors and a visualizing system, that constructs an image using the signal coming from the detectors (see also 32). [32] With the help of an electrostatic field the

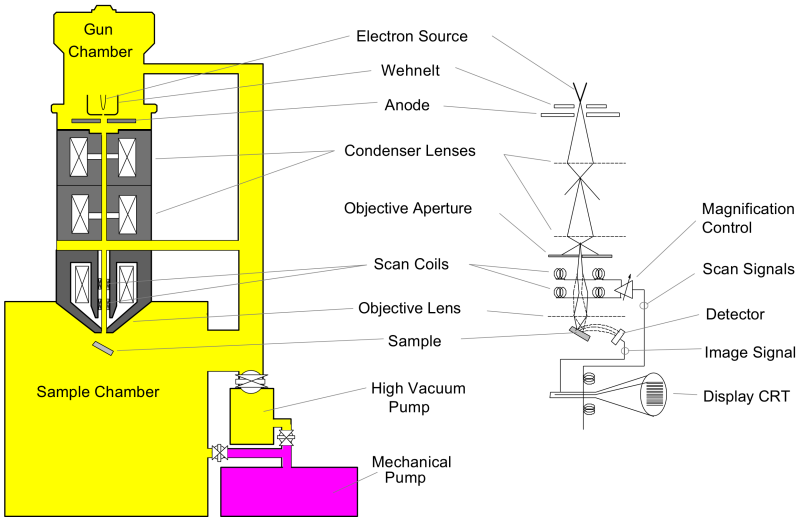

Figure 32: Schematic of an scanning electron microscope. [32]

gun accelerates the electrons down the column toward the sample. The electrons emerge as a divergent beam and a series of magnetic lenses and apertures is used to focus the beam onto the sample surface, where they interact with the atoms and produce a variety of signals, containing information about the surface, topography and

composition. The recorded image is constructed out of the detectors signals coming from the different electron-sample interactions while the beam is scanning the surface line by line. The possible interactions vary by depth where they are generated from and are depicted in fig. 33.

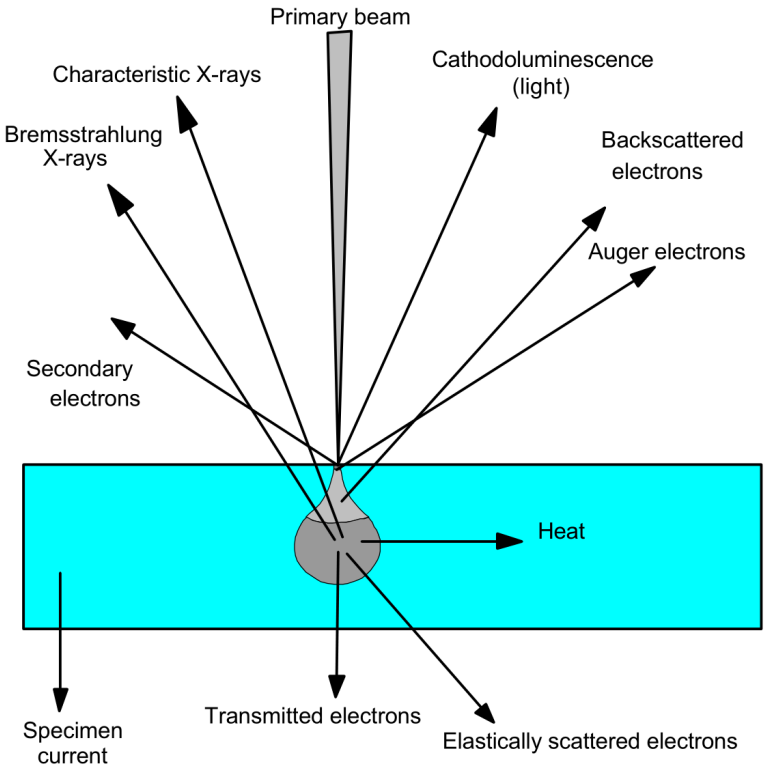

Figure 33: Possible interactions an electron can experience. [32]

9.2.1 *Environmental-SEM*

Conventional SEM's are limited by their high vacuum requirements, since samples have to be imaged under vacuum. Environmental SEM's allow samples to be observed in low-pressure gaseous environments, enabling the observation of processes such as the (de-)wetting of fibers, liquid transport and chemical reactions. This is possible due to the use of a different secondary-electron detector which is capable of operating in the presence of water vapour by the use of pressure-limiting apertures with differential pumping in the path of the electron beam to separate the vacuum region (around the gun and lenses) from the sample chamber. [32] Also the investigated samples do not have to be conductive in ESEM mode, so coating with carbon or gold is unnecessary. Specimens in this work were investigated in a Quanta 600 FEG from FEI in either low vacuum or ESEM mode. The

gaseous secondary electron detector works in a range from 1.5 Torr to 20 Torr. In this mode and with the GSED detector, wet samples can be investigated by using the Peltier cooled specimen stage. The stage is used to cool down the sample, and this with the appropriate chamber pressure, leads to condensation of water on the sample.

Part II

EXPERIMENTAL, RESULTS AND DISCUSSION

10 PLANAR THIN FILMS

10.1 TEMPERATURE RAMPS

First measurements were done using the enclosed temperature controlled stage THMS350V, and a temperature ramp, to adjust humidity below ambient conditions. To induce a change in humidity, going below ambient conditions, a temperature ramp from 25°C to 50°C was used, to lower the relative humidity in the surrounding air. Since relative humidity is temperature dependent, this leads to a desorption of water out of the polymer thin film and should therefore lead to a humidity change which corresponds to a change in relative humidity of about 20%. This is also what you can see in the plot 34, the temperature ramp induces a thickness decrease due to a humidity decrease. The measured change in thickness is only about 1%, at

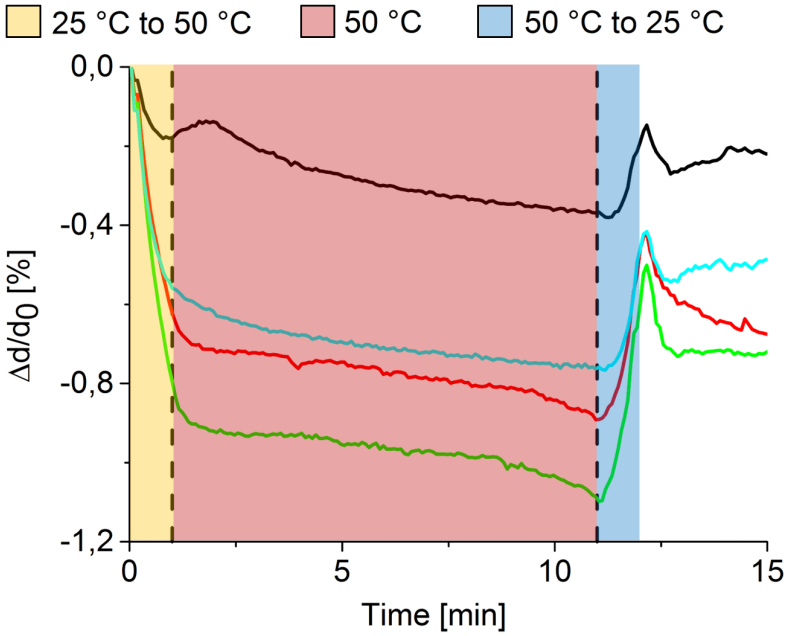

Figure 34: Relative thickness change of different samples using a temperature ramp from 25° to 50° in air.

this point this seems not much given the fact that the starting relative humidity value is at around 30% with a change of around 20% RH and later measurements will be done at even lower values. One possible explanation is that pHEMA hydrogels produce a glassy skin at the membrane-air interface for low relative humidity which protects

the film from swelling. When the humidity is low, the hydrophilic OH-terminated pendant chains of HEMA preferably orient inwards, to minimize the surface energy. This chain reorganization results in an apolar surface that swells less. [33]

10.2 THERMAL EXPANSION

Follow up measurements are performed to see if the swelling ratio is high enough for measurements in low humidity. The idea was to flood the stage with nitrogen (or any other inert gas which has 3 ppm of H_2O molecules) and again use a temperature ramp to induce small changes in humidity. For a first comparison the sample with the best (de-)swelling ratio in ambient conditions is taken and tested again in the enclosed stage flooded with nitrogen. In plot 35 measurements for ambient conditions and with a nitrogen flooded stage are shown. The two lines clearly differ and the change in thickness for the nitro-

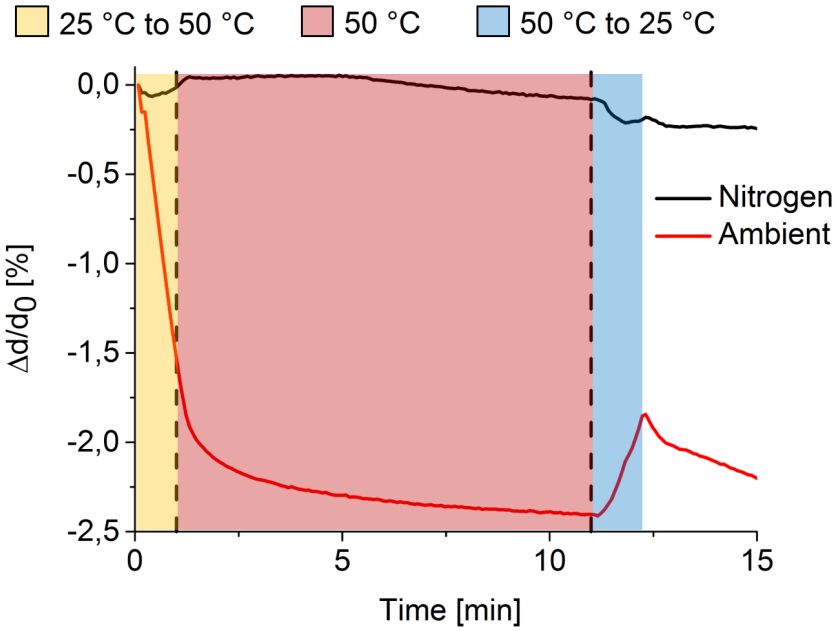

Figure 35: Relative thickness change of the same sample using a temperature ramp from 25deg to 50deg under ambient air (red) and nitrogen (black)

gen flooded stage takes on positive values. It was assumed that this is due to a thermal expansion due to the heating of the substrate and thin film. To verify that theory three samples from different depositions with different compositions were taken and analyzed, the result is depicted the plot 36. All three samples in fig. 36 show the same behaviour, no matter what deposition or composition. This means that using a nitrogen flooded chamber in combination with a temperature ramp to then change the humidity is not working out, because the

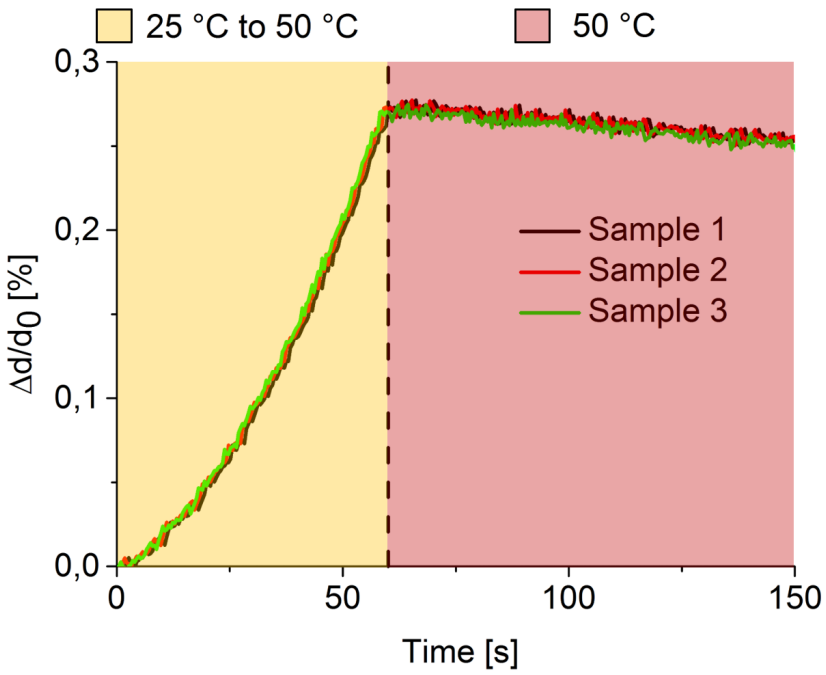

Figure 36: Relative thickness change of three samples from different depositions with different compositions using a temperature ramp from 25deg to 50deg in nitrogen.

nitrogen is too dry to additionally use a temperature ramp to change the humidity. This results lead to the construction of the custom mixing setup mentioned in section 8.

10.3 CUSTOM MIXING CHAMBER

The custom mixing setup allowed to mix dry inert gases with humidified inert gases from a bubbler and natural gas from a sample cylinder. The plots 37 (a) & (b) are measurements to test the chamber. The recorded thickness values, measured by the ellipsometer, follow the humidity values we recorded with the reference sensor quite well, although the thickness changes are very small (in the order of $< 1\%$) compared to changes around or above ambient humidity. After verifying that the custom mixing chamber is working as expected a next step is to compare different polymer compositions.

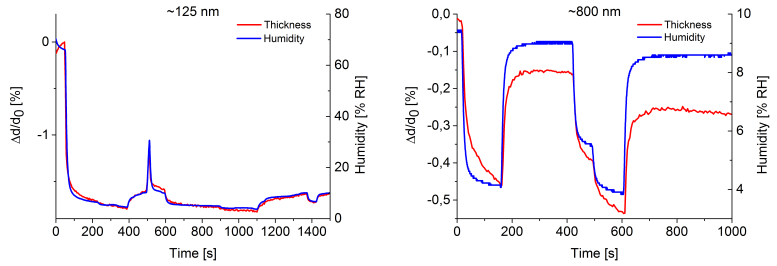

(a) (b)

Figure 37: First (a) and second (b) measurement to test the custom mixing setup.

10.4 POLYMER PERFORMANCE COMPARISON

After verifying that the setup works, as a next step a comparison of thin films with different polymer compositions is done. The following plots show four measurements where humidity is changed from 0% to 22% RH and the response over time from different polymer/hydrogel layers. Qualitatively the measured response follows quite well the curve from the reference humidity sensor for the layers without a cross-linker. What we can say from those plots is that differences in thickness and adding MAA, which should increase hydrophilicity and therefore the swelling, seems not to have much of an effect on the response, but what we can clearly see is that the response is lower if we add EGDMA as a cross-linker, which is not surprising if fig. 11 is taken into account. Also, even though the jump in humidity is quite big, only a $1-2\%$ change in thickness is measured. For the following measurements a thin film consisting of only pHEMA was used.

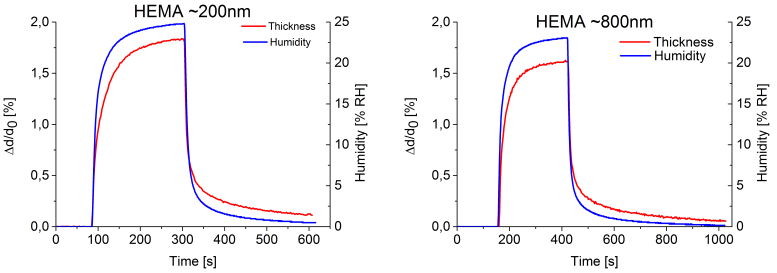

(a) (b)

Figure 38: Thickness change in percent of a pHEMA layer with 200 nm (a) and 800 nm (b) while changing the relative humidity from 0% to 22%.

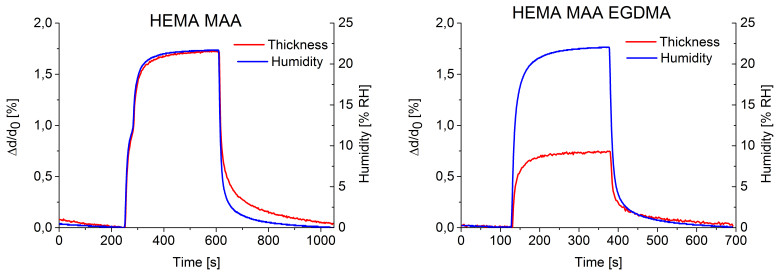

(a) (b)

Figure 39: Thickness change in percent of a p(HEMA-co-MAA)(a) and a EGDMA cross-linked p(HEMA-co-MAA) (b) layer while changing the relative humidity from 0% to 22%.

10.5 NATURAL GAS

First measurements were done as a test to see if there is a response from the thin film in a natural gas environment. To do this the stage was flooded with inert gas (grey), to then see an increase in thickness when the natural gas flow starts, which has a higher relative humidity. As you can see in the plot 40 it's clearly visible when the natural gas flow (blue) starts.

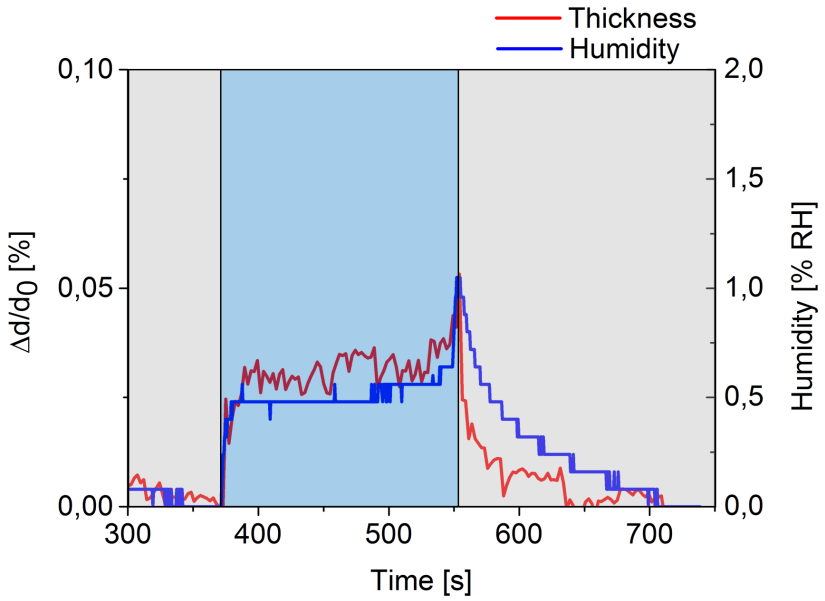

Figure 40: First measurement to see if there is a measurable response from the polymer film when a natural gas flow (blue) starts.

10.6 DIFFERENT HUMIDITY LEVELS

Since the last measurements showed that there is a good response from the thin film in a natural gas environment, the question now is, if there is also a measurable difference for the different humidity levels in natural gas. For this, three natural gas sample cylinders were provided, filled with natural gas with different levels of humidity (Gas Nr. 1: unknown, Gas Nr. 2: 0,11%RH, Gas Nr. 3: 0,57%RH, values obtained from dew point measurements). The cylinders were simply (ex)changed during the measurement, starting with Nr. 1, while the pressure/flow rate was held constant for the different cylinders. The start of the different flows is clearly distinguishable in fig. 41. The first three blocks (blueish color) are natural gas samples with different levels of humidity and the last one (grey) is nitrogen. Also, again the thin film thickness does not change much compared to above ambient conditions, but it is measurable and even in this range the swelling is high enough to detect different levels of humidity. Since the reference sensor has an error of about 4% in this region [7] the absolute values we get are not comparable with what is known for the natural gas samples. But the relative differences of around 0,5%RH is in good comparison to the real value of 0,46%RH.

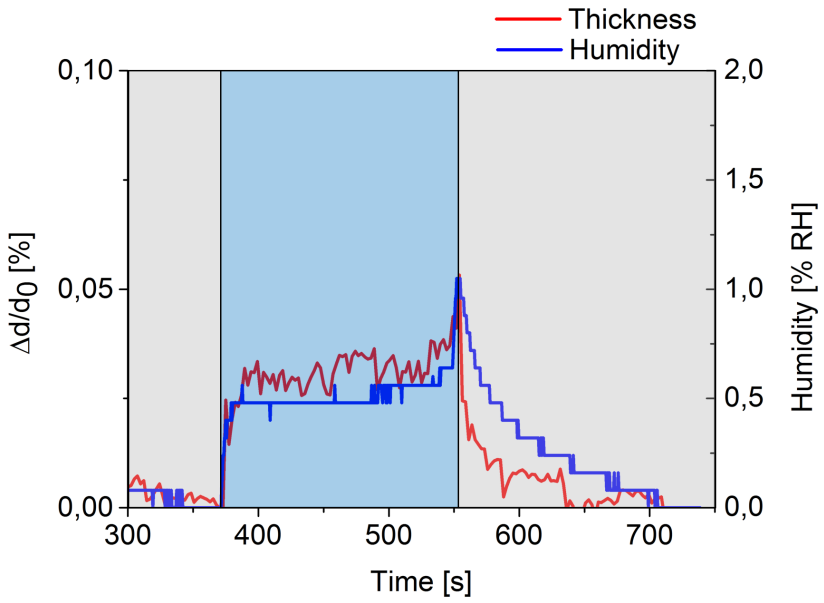

Figure 41: Measurement to see if there is a visible difference for the different humidity levels occuring in natural gas.

11 NANO-STRUCTURING

11.1 INTRODUCTION

The swelling of a thin film is constrained by the attachment to the surface from which they are grown. The use of nanostructures reduces those geometrical constraints, increasing the surface area to overcome the glassy skin effect and lower diffusion effects.[1] This should lead to a greater overall water uptake, enabling a higher degree of swelling. From the paper of Ince et al. [1] the idea of creating a hydrogel nanotube forest using templates emerged. In the paper it is stated that the water uptake changed from 10-17% to 60-78% weight increase, due to the lager surface area-to-volume ratio of the nano-tubes compared to the planar films, which can be seen in plot 43.

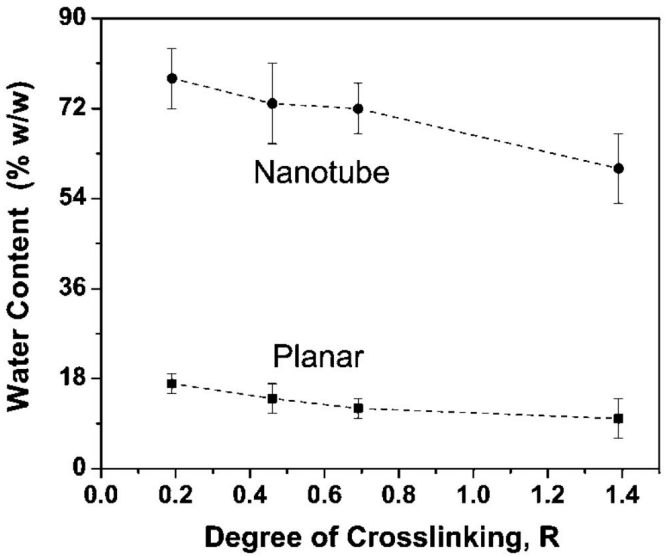

Figure 42: Water content of planar films in comparison to nano-structured films over different crosslinking ratios. [1]

11.2 AAO TEMPLATES

To be able to create a hydrogel nano-tube forest, templates are needed to, as a first step, deposit the polymer thin film onto. Anodized aluminum oxide, short AAO, membranes serve as excellent templates, because AAO is self-organized with a honeycomb-like structure, formed by high density arrays of uniform and parallel nanopores. Their di-

ameter can be controlled with great precision and their pore length can range from tens to few hundred micrometers. [34] The membranes (Anodisc 25, Whatman) used in the experimental part have a hole diameter of below or around 200 nm. With iCVD and a low $\frac{P_m}{P_{sat}}$ value one can still get a conformal polymer thin film inside the pores, building either nano-rods or even hollow, tube-like structures, depending on the thickness of the deposited polymer film. In the picture on the bottom you can see a schematic of such an AAO membrane and an SEM image of what was expected in terms of uniformity and distribution of the pores.

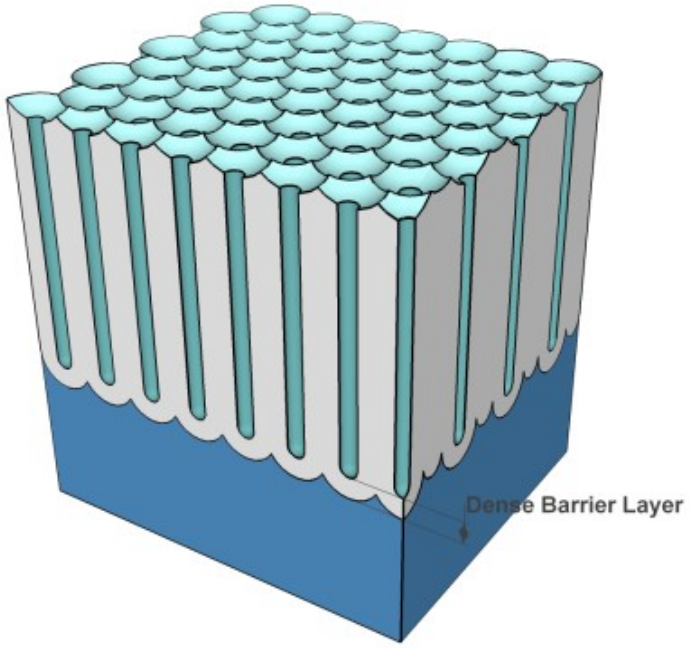

Figure 43: Schematic of a cross section of an AAO membrane. [35]

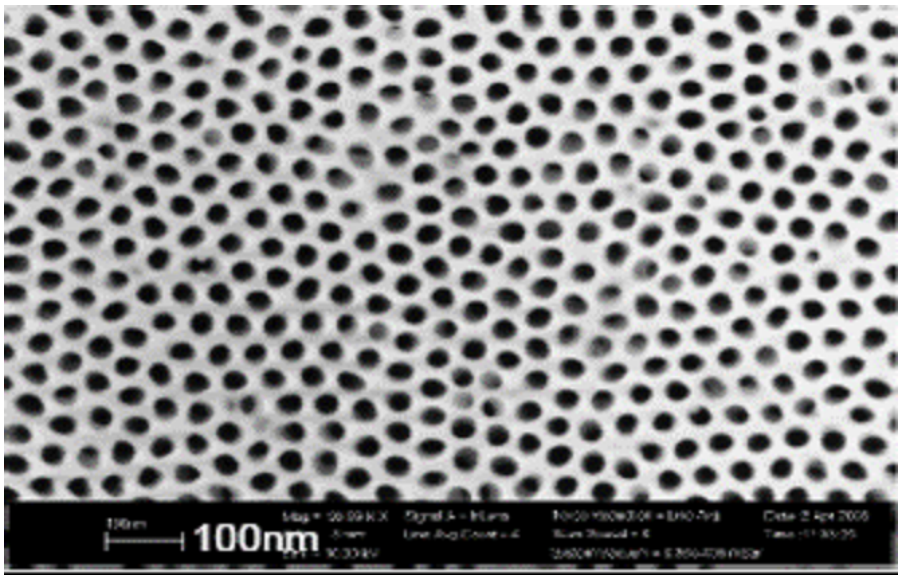

Figure 44: SEM image of what the surface of the AAO membrane is expected to look like in terms of the nano pores. [36]

11.3 ETCHING

After the deposition of the polymer onto the template, the polymer thin film should conformaly coat the top and inside of the pores. To end up with free standing nano-tubes, the template needs to be removed without damaging the polymer film. There are different methods to get rid of the template, but one of the easiest methods and the one used in this thesis is wet etching, where an acid, like hydrochloric acid or a base like sodium hydroxide, is used to etch away the aluminium membrane. For this the template coated by the polymer thin film needs to be fully submerged in a solution and since pHEMA, without a crosslinker, is not stable in an aqueous environment, the thin film could dissolve. But with an increasing crosslinker ratio in the polymer film composition the swelling ratio decreases. Since it is not known at this point which effect is greater EGDMA was added to the composition as a crosslinker to produce nanotubes in a first step. The whole process works then as follows, the first step is the deposition of the thin film with the desired composition per iCVD onto the AAO template. Then the template is flipped onto a substrate and secured with carbon tape. The template is then put into a solution with hydrochloric acid, until the aluminium has been (partially) etched away from the "bottom side".
Figure 45 is an example out of the paper from Ince et al. [1] and represents expectations on what the outcome could look like.

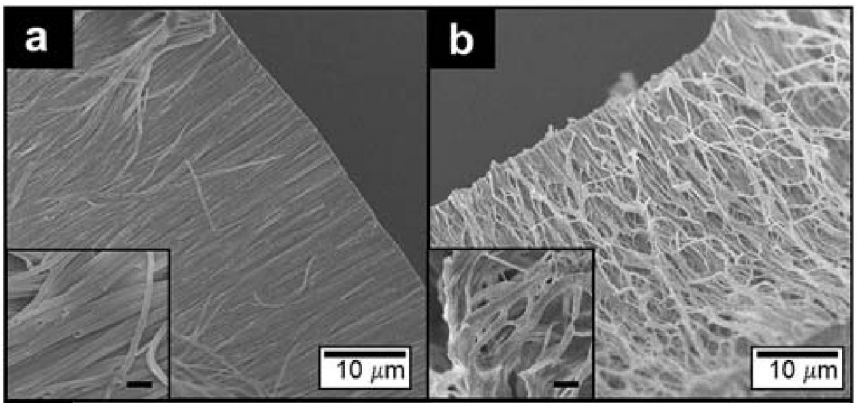

Figure 45: Expectations on what the nanotubes look like after the AAO membrane has been etched away in the dry (left) and swollen (right) state. [1]

11.4 ANALYSIS

Up until now spectroscopic ellipsometry has been used to analyse the deposited thin films, but since ellipsometry can't be used to measure any quantitative values on nano-structured materials with satisfying results, only qualitative analysis was done. For this atomic force microscopy and scanning electron microscopy (see 9) were used.

11.4.1 *AAO membrane*

Since there is an AFM available in-house it was first tried to use the AFM for taking images of the AAO membrane, fig. 46 (a), but since the outcome did not match our expectation, SEM images (in-house see fig. 46 (b), and in cooperation with the FELMI fig. 46 (c)-(d)) have been taken in addition. If the images in fig. 46 are compared to fig. 44, it can be seen that the shape of the pores and the pore diameter distribution are not as uniformly as thought. This could lead to earlier clogging of the single pores if the $\frac{P_m}{P_{sat}}$ value is not low enough.

11.4.2 *Different etching times*

Figure 47 shows a SEM image of a partially etched template (16 hours) with a thin film deposited inside the pores. Not all pores seem to be filled and there the walls of the aluminium pores are still visible around the hydrogel, leaving us with nano-bumps rather than nanotubes.
The next sample, shown in figure 48, has been etched for 25 hours. It seems that there are no aluminium pores visible on first sight and the surface seems to have a top layer that looks wrinkled and cracked.

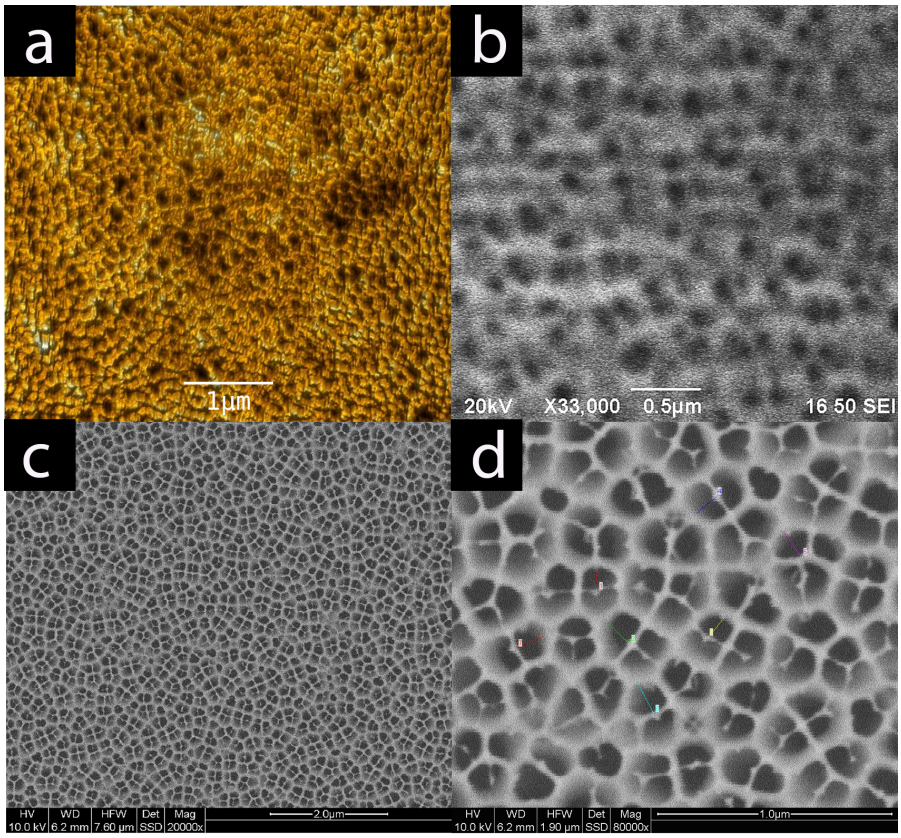

Figure 46: AFM (a) and SEM (b)-(d) images taken of the AAO membrane.

If we zoom in into one of those cracks, rod-like structures are visible that resemble the nano-tubes from fig. 45. A visual guideline has been added to the figure in the left lower corner. The image shows a view from the top.

11.4.3 *Cross Section*

In figure 49 a cross section of the template etched for 25 hours is shown. This cross section was not intended and is a result from the rigid template breaking under stress. The image suggests, that there is still a big part of the aluminum pores left, as those structures seem hollow, stiff and highly periodically. The pores seem to be only partially filled with pHEMA and it looks like if there is a top layer as seen in fig. 48. The partial filling suggests that there is clogging of the pores due to a $\frac{P_m}{P_{sat}}$ value that is too high.

11.4.4 *EDX Spectra*

To verify that the structures seen in fig. 49 are in fact aluminum pores energy dispersive x-ray spectroscopy inside the SEM was used. Three measurements were done, one for a AAO template without deposi-

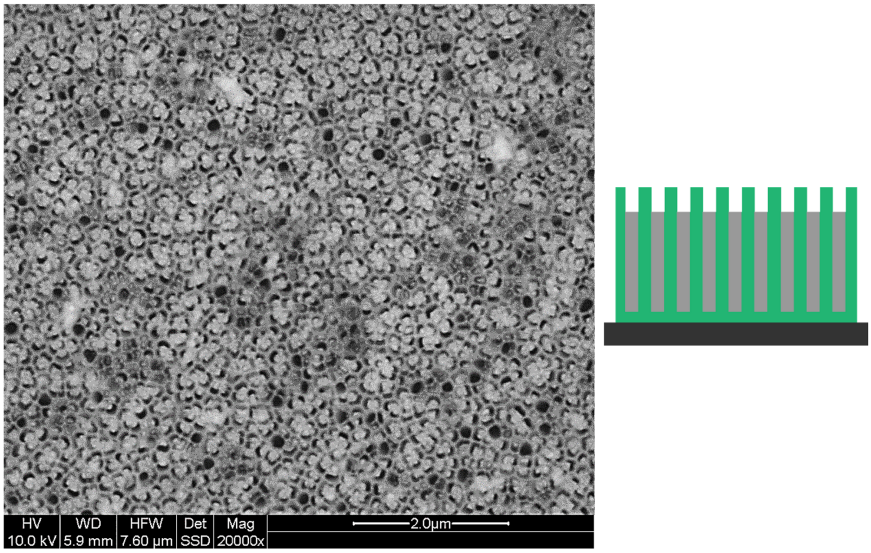

Figure 47: SEM image of a partially etched template with a polymer thin film deposited inside the pores. On the right a visual guide is shown that indicates the polymer in green and the aluminium in gray.

tion, and two for a sample with a thin film deposited onto and after etching, using different penetration depths. The respective results are shown in fig. 50 from left to right. There is an aluminium peak in all three spectra to see, which means, that there is still aluminium present in all of the samples, and therefore the aluminium has only been partially etched away by the hydrochloric acid bath. There is also a chlorine peak visible in the spectra with etching, which is a residue from the hydrochloric acid since the samples are not washed out after the etching process. Also a carbon peak is visible that stems from the deposited polymer film.

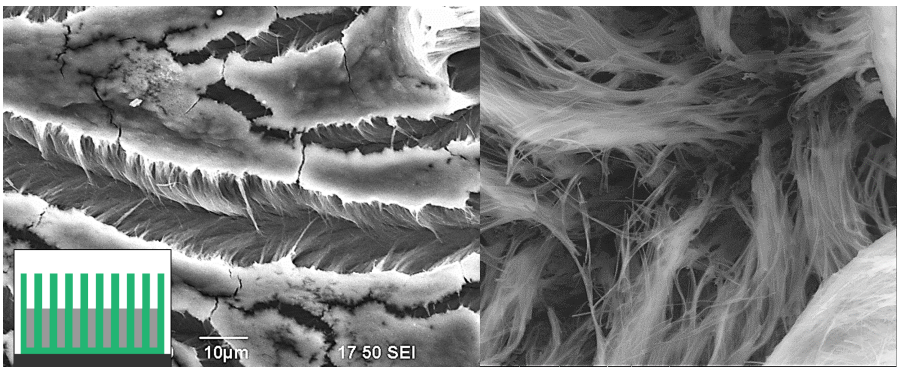

Figure 48: SEM image of a sample etched for ~25h with a visible top layer (left), a zoomed in view with rod-like structures (right). In the left lower corner a visual guide is shown that indicates the polymer in green and the aluminium in gray.

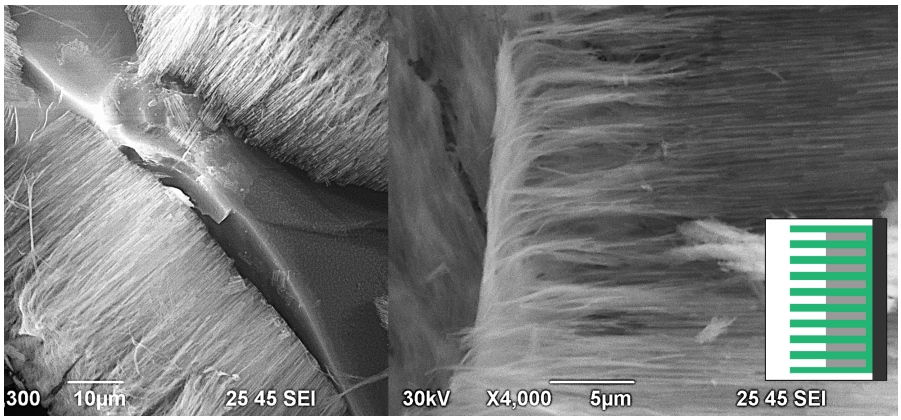

Figure 49: SEM image of a cross section of a sample etched for 25 hours with partially filled pores. In the right lower corner a visual guide is shown that indicates the polymer in green and the aluminium in gray.

11.4.5 *AFM Measurements*

An attempt was made to use atomic force microscopy to image the swelling of a single nanotube. Those measurements have been done in collaboration with Prof. Christian Teichert from the Montanuniversität Leoben, with an AFM placed in a humidity chamber to be able to regulate humidity. The results are shown in fig. 51. Due to the fact, that there is always some kind of drift and the surface changes, the images are taken on roughly the same spot rather than the exact same spot on the same sample with a relative humidity of 30% and 65%. The sample is the same as in fig. 47 and there are also no single nano-tubes distinguishable in the images in fig. 51. It seems if the structures are bump-like, which is in agreement with what is deducted from fig. 47. At a lower relative humidity (fig. 51, left), the surface is dominated by dot-like surface features with a diameter of around (120 +/- 30) nm and (30 +/- 10) nm in height, compared to that, these dots are smaller with a diameter of (90 +/- 15) nm and a height of (7 +/- 2) nm at 65% RH (fig. 51, right). The size of the surface features decreases with higher relative humidity. Also the values for the roughness in figure 52 are higher for 30% of relative humidity. The imaging could be done again with a fully etched sample, but the results suggest that at 65% RH, most of the surface is already gel-like and very soft and/or there is water on the surface, making it difficult to capture the swelling of a single nano-tube.

11.4.6 *Environmental SEM*

Due to the unrewarding experience with AFM, a different approach was to use environmental scanning electron microscopy to capture the swelling of the nano-structured film. This was done in collabo-

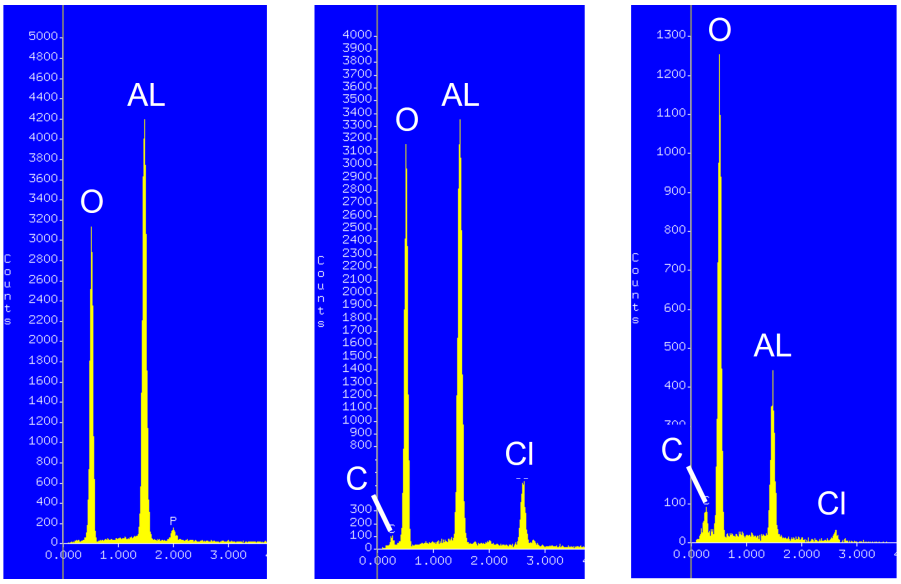

Figure 50: EDX Spectra from the template without deposition (left), the AAO template with a thin film deposited onto and after etching (middle), the AAO template with a thin film deposited onto, after etching and with a lower penetration depth (right).

ration with Dr.techn. Zankel at the Institute of Electron Microscopy and Nanoanalysis in Graz. The images are taken on a Quanta 600 FEG in „ESEM“ mode with the imaging gas being water vapour. The pressure range in this mode is from 1.5 Torr to 20 Torr and a gaseous secondary electron detector (GSED) is used. This mode enables the use of wet samples and also the imaging of a (de-)wetting process by changing the sample temperature or pressure. The following figures show images of the sample surface at different magnifications taken before/in the wet state and after drying again.

Figures 53 and 54 show the same spot on the sample before wetting and after drying. There are no major visible differences nor have any

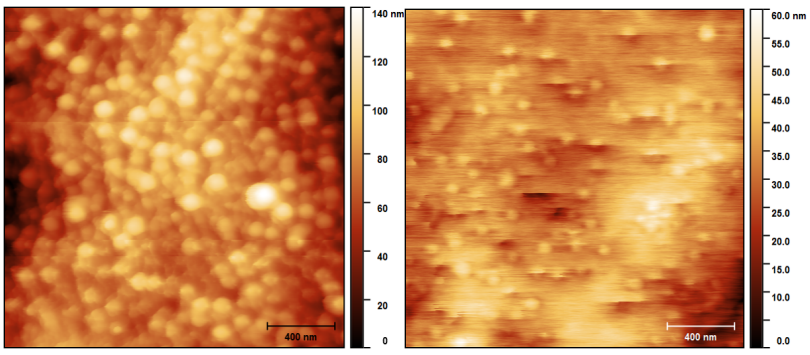

(a) (b)

Figure 51: AFM image of a template coated with a polymer film taken at a relative humidity of about 30% (a) and 65% (b).

Relative humidity	RMS roughness σ /nm		
	5 x 5 µm²	2 x 2 µm²	1 x 1 µm²
65 % RH	24.65 ± 7.85	9.80 ± 3.80	5.90 ± 1.15
30 % RH	110.10 ± 2.70	21.45 ± 1.45	13.60 ± 1.20

Figure 52: Calculated roughness from an AFM image for 30% and 65% RH.

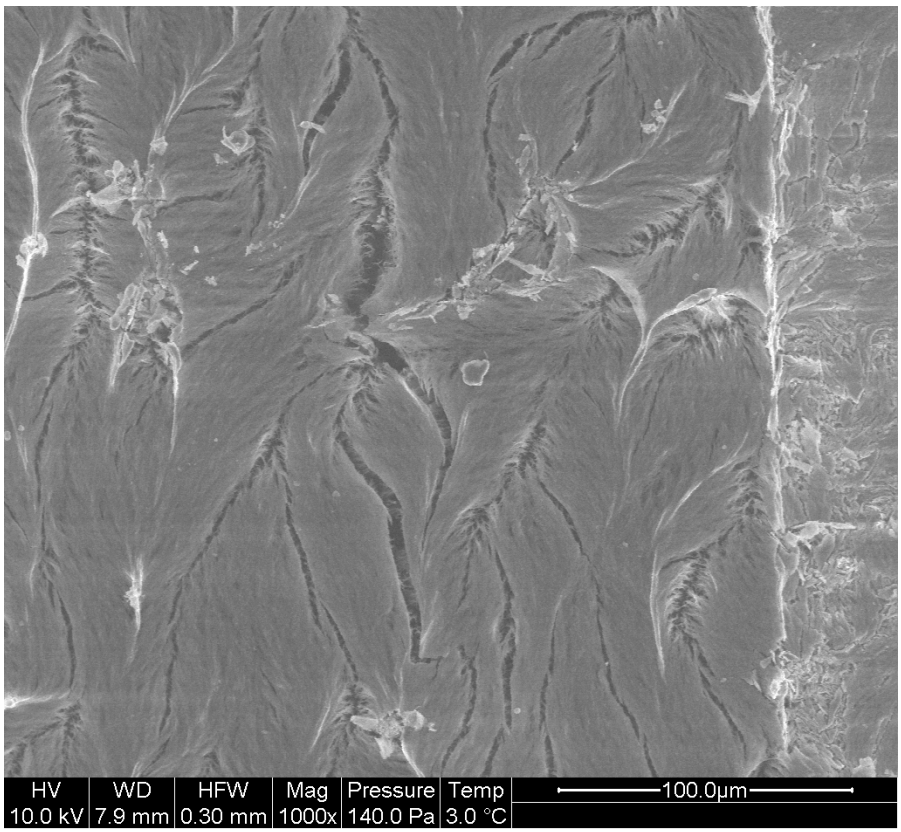

Figure 53: SEM image overview of the sample surface before wetting

new cracks formed which suggests that there was only little swelling involved leading to mechanical stress or strain. Figures 55 and 56 show a zoomed in view of the spot while wetting and after drying again. Even while water is present, and the cracks and trenches are filled, there is only very little swelling visible. Since this would involve the increase in thickness in all directions, leading to a topographical change and also a change in the working distance of the SEM it is deducted that the degree of cross-linking is too high for a qualitative analysis in the ESEM.

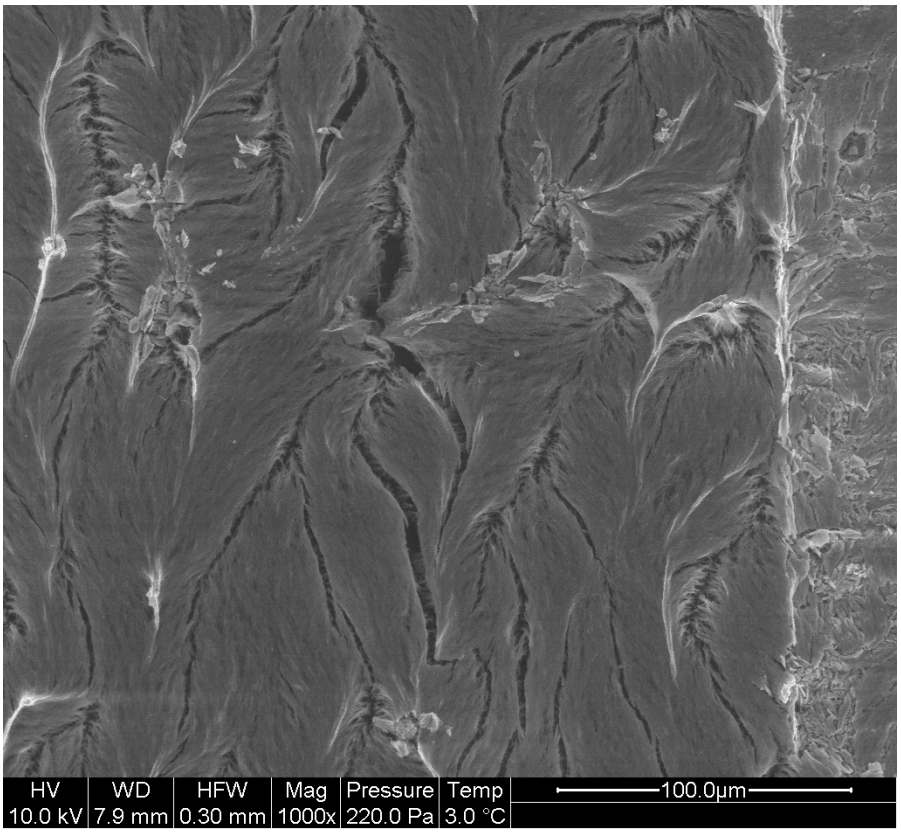

Figure 54: SEM image overview of the sample surface after wetting

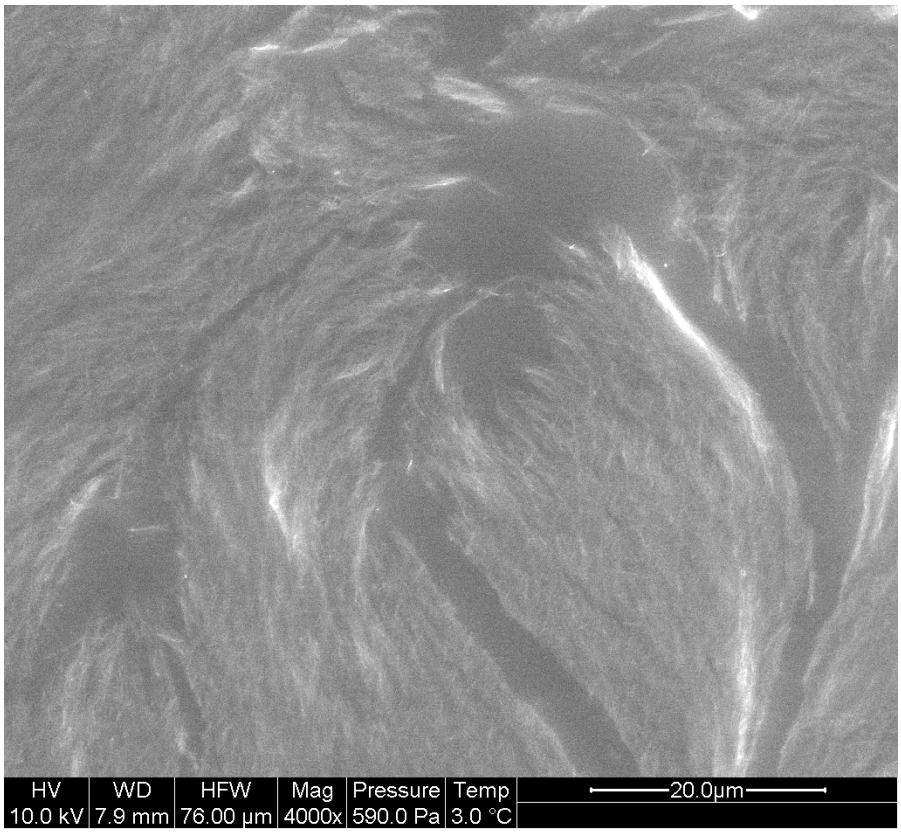

Figure 55: SEM image of the sample surface zoomed in in the wet state

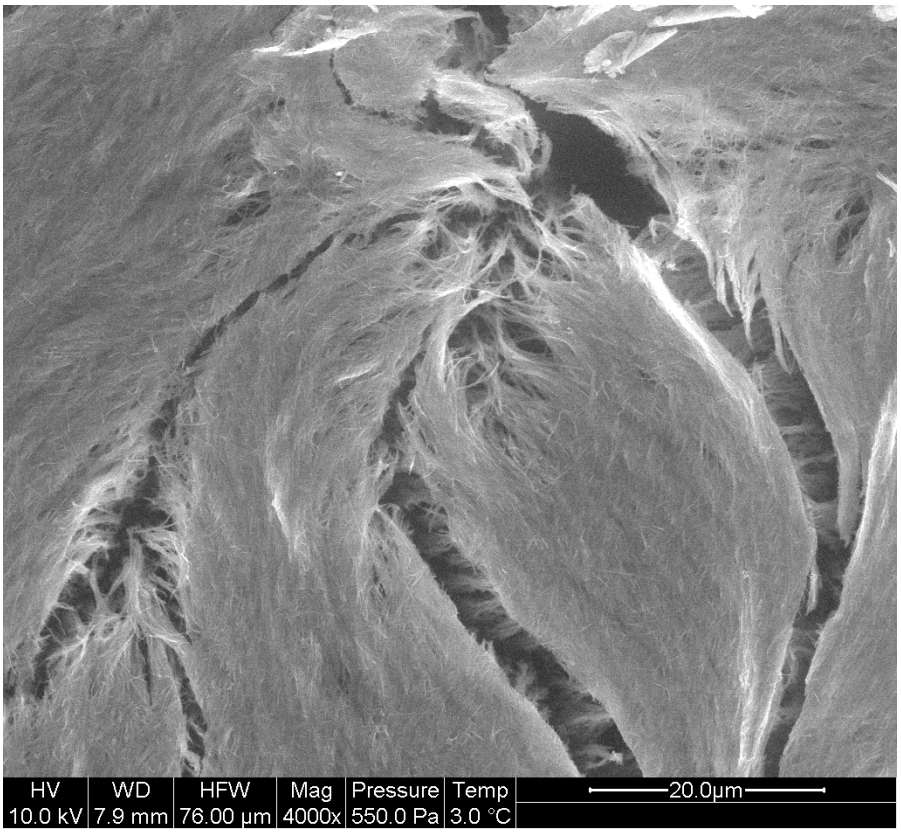

Figure 56: SEM image of the sample surface zoomed in after wetting

12 CONCLUSION AND OUTLOOK

12.0.1 *Planar thin films*

The use of temperature ramps to control the humidity inside the enclosed stage of the ellipsometer works for ambient conditions (fig. 34), but has been unsuccessful with the use of inert gas, because the increase of sample thickness due to thermal expansion is then higher than the measurable thickness increase due to the change in humidity (fig. 35 and 36).
The custom built mixing chamber is shown to be working in the desired range from 0% relative humidity to up to 95% relative humidity and can be used for upcoming projects (see fig. 37).
A comparison between co-polymer thin films consisting of pHEMA with 200 nm and 800 nm thickness, p(HEMA-co-MAA) and a EGDMA cross-linked p(HEMA-co-MAA) shows that the thickness of the polymer film and adding methacrylic acid to the composition is not changing the relative thickness increase when going from 0% to 22% of relative humidity (fig. 38 and 39). Adding EGDMA as a cross-linker to the composition changes lowers the response drastically.
First measurements in a natural gas environment showed a clear response from the hydrogel when the flow starts and different levels of humidity normally occurring in natural gas can be distinguished (fig. 40 and 41). For further analysis dessicant saturation measurements should be done, to see if the polymer films are immune to saturation.

12.0.2 *Nano-structuring*

Qualitative analysis shows the successful synthesis of nano-structured films with the help of anodic aluminium oxide membranes as templates for the polymer. 16 hours of etching in 1 molar hydrochloric acid only leads to partial etching of the aluminium oxide leaving nano-bumps rather than tubes or rods, which can be seen in figure 47. In figure 48 the structures seem more tube like with 25 hours of etching, but figure 49 suggests that there is still aluminium left, which is later backed up by the EDX measurements shown in 50. Atomic force microscopy has been unrewarding as a method to measure the swelling of a single nano-tube in-situ because of the gel-like surface 51. Imaging the swelling of the nano-structured polymer film via an evironmental SEM did not show the desired results (fig. 53-56), suggesting that the cross-linking ratio is too high for a qualitative analysis of the swelling behaviour.

BIBLIOGRAPHY

[1] Gozde Ozaydin Ince, Gokhan Demirel, Karen K. Gleason, and Melik C. Demirel. "Highly swellable free-standing hydrogel nanotube forests." In: *Soft Matter* 6.8 (2010), p. 1635. DOI: 10.1039/c000569j.

[2] Seungjun Baek, Juwon Min, and Jae W. Lee. "Equilibria of cyclopentane hydrates with varying HLB numbers of sorbitan monoesters in water-in-oil emulsions." In: *Fluid Phase Equilibria* 413 (2016), pp. 41–47. DOI: 10.1016/j.fluid.2015.10.018. URL: http://ars.els-cdn.com/content/image/1-s2.0-S0378381215301783-gr1.jpg.

[3] A V Arundel, E M Sterling, J H Biggin, and T D Sterling. "Indirect health effects of relative humidity in indoor environments." In: *Environmental health perspectives* 65 (1986), pp. 351–361. ISSN: 0091-6765.

[4] Hamid Farahani, Rahman Wagiran, and Mohd Hamidon. "Humidity Sensors Principle, Mechanism, and Fabrication Technologies: A Comprehensive Review." In: *Sensors* 14.5 (2014), pp. 7881–7939. DOI: 10.3390/s140507881.

[5] G. J. Symons. "A contribution to the history of hygrometers." In: *Quarterly Journal of the Royal Meteorological Society* 7.39 (2007), pp. 161–185. DOI: 10.1002/qj.4970073902.

[6] Zhi Chen and Chi Lu. "Humidity Sensors: A Review of Materials and Mechanisms." In: *Sensor Letters* 3.4 (2005), pp. 274–295. DOI: 10.1166/sl.2005.045.

[7] Sensirion. *SHT1x Datasheet*. Sensirion. URL: https://www.sparkfun.com/datasheets/Sensors/SHT1x_datasheet.pdf.

[8] Stanislav Kolpakov, Neil Gordon, Chengbo Mou, and Kaiming Zhou. "Toward a New Generation of Photonic Humidity Sensors." In: *Sensors* 14.3 (2014), pp. 3986–4013. DOI: 10.3390/s140303986.

[9] Yu-Cheng Lin. "Breath sensor based on reflective optical lensed fiber." In: *Microwave and Optical Technology Letters* 55.2 (2012), pp. 450–454. DOI: 10.1002/mop.27322.

[10] Lina Xu, Joseph C Fanguy, Krunal Soni, and Shiquan Tao. "Optical fiber humidity sensor based on evanescent-wave scattering." In: *Optics letters* 29 (11 2004), pp. 1191–1193. ISSN: 0146-9592.

[11] Yao Lin, Yuan Gong, Yu Wu, and Huijuan Wu. "Polyimide-coated fiber Bragg grating for relative humidity sensing." In: *Photonic Sensors* 5.1 (2014), pp. 60–66. DOI: 10.1007/s13320-014-0218-8.

[12] Jinesh Mathew, Yuliya Semenova, and Gerald Farrell. "A high sensitivity humidity sensor based on an Agarose coated photonic crystal fiber interferometer." In: *OFS2012 22nd International Conference on Optical Fiber Sensors*. Ed. by Yanbiao Liao, Wei Jin, David D. Sampson, Ryozo Yamauchi, Youngjoo Chung, Kentaro Nakamura, and Yunjiang Rao. SPIE, 2012. DOI: 10.1117/12.975153.

[13] M. Consales, A. Buosciolo, A. Cutolo, G. Breglio, A. Irace, S. Buontempo, P. Petagna, M. Giordano, and A. Cusano. "Fiber optic humidity sensors for high-energy physics applications at CERN." In: *Sensors and Actuators B: Chemical* 159.1 (2011), pp. 66–74. DOI: 10.1016/j.snb.2011.06.042.

[14] Jacob Fraden. *Handbook of Modern Sensors*. Springer International Publishing, 2016. DOI: 10.1007/978-3-319-19303-8.

[15] John M. Wallace and Peter V. Hobbs. *Atmospheric Science: An Introductory Survey*. Academic Press, 2006. ISBN: 9780080499536.

[16] Hanno Schaumburg, ed. *Sensoranwendungen*. Vieweg,Teubner Verlag, 1995. DOI: 10.1007/978-3-322-96721-3.

[17] *Chemical structure of polyethylene*. URL: https://upload.wikimedia.org/wikipedia/commons/4/45/Polyethylene_repeat_unit.svg.

[18] *Chemical structure of polystyrene*. URL: https://upload.wikimedia.org/wikipedia/commons/6/60/Polystyrene.svg.

[19] *Chemical structure of acrylnitril butadien styrol*. URL: https://commons.wikimedia.org/wiki/File:Acrylnitril-Butadien-Styrol-Copolymer.svg.

[20] H. Schaumburg. *Werkstoffe und Bauelemente der Elektrotechnik: Polymere*. Vol. 6. H. Schaumburg, 1997.

[21] Karen K. Gleason, ed. *CVD Polymers*. Wiley-VCH Verlag GmbH & Co. KGaA, 2015. DOI: 10.1002/9783527690275.

[22] Polymer Science Learning Center. *Crosslinking*. URL: http://pslc.ws/macrog/xlink.htm.

[23] Gehong Su, Tao Zhou, Yanyan Zhang, Xifei Liu, and Aiming Zhang. "Microdynamics mechanism of D2O absorption of the poly(2-hydroxyethyl methacrylate)-based contact lens hydrogel studied by two-dimensional correlation ATR-FTIR spectroscopy." In: *Soft Matter* 12.4 (2016), pp. 1145–1157. DOI: 10.1039/c5sm02542g.

[24] Karen K. Gleason. *Reactor Schematic*. URL: http://web.mit.edu/gleason-lab/Images/ReactorSchematic2b.jpg.

[25] *Chemical structure of DI, tert-Butyl peroxide*. 2018. URL: https://www.sigmaaldrich.com/content/dam/sigma-aldrich/structure7/108/mfcd00008803.eps/_jcr_content/renditions/mfcd00008803-large.png.

[26] *Chemical structure of ethylene glycol dimethacrylate*. URL: https://www.sigmaaldrich.com/content/dam/sigma-aldrich/structure0/131/mfcd00008590.eps/_jcr_content/renditions/mfcd00008590-large.png.

[27] *Chemical strucutre of hydroxyethyl methacrylate*. URL: https://www.sigmaaldrich.com/content/dam/sigma-aldrich/structure1/139/mfcd00002863.eps/_jcr_content/renditions/mfcd00002863-large.png.

[28] *Chemical structure of methacrylic acid*. URL: https://www.sigmaaldrich.com/content/dam/sigma-aldrich/structure4/061/mfcd00002651.eps/_jcr_content/renditions/mfcd00002651-large.png.

[29] Paul Salzmann. "Preparation of smart thermo-responsive polymer thin films by initiated chemical vapor deposition." MA thesis. Graz University of Technology, 2017.

[30] Hiroyuki Fujiwara. *Spectroscopic Ellipsometry: Principles and Applications*. Wiley, 2007. ISBN: 9780470016084.

[31] *AFM operating principle*. URL: https://www.nanosurf.com/images/support/afm-modes-afm-operating-principle.png.

[32] Philips Electron Optics. *ENVIRONMENTAL SCANNING ELECTRON MICROSCOPY - An Introduction to ESEM ®*. 1996.

[33] Katrin Unger, Roland Resel, and Anna Maria Coclite. "Dynamic Studies on the Response to Humidity of Poly (2-hydroxyethyl methacrylate) Hydrogels Produced by Initiated Chemical Vapor Deposition." In: *Macromolecular Chemistry and Physics* 217.21 (2016), pp. 2372–2379. DOI: 10.1002/macp.201600271.

[34] *Nanoporous Anodic Aluminum Oxide*. URL: http://www.inredox.com/technology/anodic-aluminum-oxide/.

[35] *AAO on Al Cross-Section*. 2018. URL: http://www.inredox.com/wp-content/uploads/2015/03/AAO-Cross-Section-w-Al-2-495x400.jpg.

[36] Prof. Dr. Peter Lemmens. *SEM Images of Nanoporous Anodic Aluminum Oxide*. URL: http://www.peter-lemmens.de/images/light-1.GIF.